U.S. DEPARTMENT OF THE INTERIOR

U.S. GEOLOGICAL SURVEY

Comparison of Sea-ice and Glacial-ice Rafted Debris: Grain Size, Surface Features, and Grain Shape

By

Gita Dunhill

Open-File Report 98-367

Menlo Park, California

1998

Abstract

Grains that have been transported and released by drifting ice floes (sea ice) and grains that have been transported and deposited by icebergs differ only slightly in terms of grain size and shape, but have extremely different surface features. Grain-size analysis shows that icebergs transport and deposit generally coarser, more poorly sorted material than does sea ice. Grain shape analysis suggests that medium to very fine sand grains of quartz entrained into sea ice tend to have a more elongate form with rounded edges, while iceberg-rafted quartz grains have a more spherical form with angular edges. These differences, however, are too subtle to reliably identify the ice transport mechanism. However, the analysis of surface features under a scanning electron microscope (SEM) suggests that the two sediment types can be differentiated by the abundance or absence of specific groups of surface features. The surfaces of glacial grains are dominated by mechanical breakage features such as high relief, breakage blocks, conchoidal fractures, and step-fractures, while the surfaces of sea-ice grains have an abundance of chemical features such as pitted surfaces and show evidence of silica dissolution, precipitation, and oriented etching pits. Identification of sea-ice-rafted debris (SIRD) and glacial-ice-rafted debris (IRD) in deep sea deposits has important climatic implications.

Acknowledgments

I would like to thank Mike Mullens and Larry Phillips for providing the sea floor and glacial samples. Nancy Smith and Don Pardo were invaluable in helping with the SEM sessions. The careful reviews of Dietz Warnke and Sue Hershfeld improved this thesis. Finally, I'd like to thank Erk Reimnitz least of all for his sea ice samples, but more for his support and mentoring on this project from its conception to completion.

Table of Contents

List of Figures

List of Tables

List of Plates

List of Appendices

Introduction

The ability to identify sea ice sediment has two major geologic implications. First, being able to identify grains that have been transported by drifting sea ice would help clarify the sediment budget of the Arctic basin. It would increase our understanding of the processes involved in transporting sediment from the shelf areas into the interior of the Arctic basin. Secondly, knowledge of the type of ice transport mechanism responsible for bringing sediment into the basin (sea ice versus glacial ice) would help in interpreting the type of ice regime operating at a specific time. More specifically, knowledge regarding the prevalent ice regime has climatic implications because the amount and type of ice present at high northern latitudes record the Arctic region's climate. The varying intensity and contribution of sea ice rafting versus iceberg rafting represent changing climatic conditions.

For example, a large decrease in the amount of sea ice rafted sediment may indicate less open water conditions and less movement and melting of sea ice These conditions may represent a thicker and tighter ice cover which would suggest a colder climate in the Arctic ocean (Clark et al., 1980).

Background

Sedimentation process

Iceberg and sea ice rafting are only two of the many depositional processes that have been active on the Arctic Ocean's sea floor. The depositional processes involved in the Beaufort Sea include transport of sediments by:

1. sea ice rafting
2. glacial rafting
3. turbidity currents
4. aeolian activity

5. currents carrying river deposits

(Thiede et al., 1990).

Based upon textural data, most modern Arctic sedimentation (the last 5 m.y.) is attributed to either icebergs or sea ice (Clark et al., 1980). The modern Arctic Ocean is covered by perennial ice of which about 99% is frozen sea water known as pack ice or sea ice. Icebergs make up the remaining 1% (Clark et al., 1980).

Iceberg Rafting

The glaciers in the Arctic Ocean come from the islands of Arctic Canada (primarily Ellesmere Island), the Siberian coast where icebergs calves off glaciers located on offshore islands including Franz Josef Land, Severnaya Semlya, and Bennett Island, and from northern Greenland and Svalbard (Clark, 1990). Icebergs which originate as glaciers and shelf ice carry a significant sediment load which gets delivered to the sea floor during summer months when the glaciers begin to melt and streams of sediment-laden runoff release sediment. Sediments range from boulder size to fine-grained silt and clay (Clark, 1990).

Sea Ice Rafting

For SIRD to be found in the Central Arctic basin, sediment-laden ice must have survived transport away from the basin margin to the basin interior. Sediment is incorporated into Arctic sea ice along the shelves of the ocean basin margins primarily by suspension freezing (Kempema et al., 1993). Suspension freezing occurs when strong waves, currents and ice wallow generate turbulence during ice formation and resuspend sediment from the shallow bottom, allowing it to be incorporated into newly forming frazil ice (ice crystals suspended in water) or slush ice. Small sedimentary particles lifted by frazil off the sea bed together with those scavenged by frazil ice from the water column can produce very high loads of suspended matter (Reimnitz et al., 1992). Anchor ice forms when ice crystals attach to the shallow bottom in subfreezing temperatures where they adhere to coarse particles or to each other. When anchor ice is sufficiently buoyant it rises to

the surface and carries the sediment with it. Figure 1 shows anchor ice adhering to the substrate. This process is capable of entraining very coarse material into sea ice (Reimnitz et al., 1992). The relative contributions of these two ice transport mechanisms (sea ice versus iceberg) to the sedimentation of the basin remain unknown.

Previous Work

Research cited in this section relates to this thesis in one of three ways: a) work on glacially derived sediment, b) research on sea ice sediment or c) research using surface features and/or grain shape to determine transport or depositional histories.

a) Iceberg-Rafted Debris

Previous work has focused on determining the characteristics of iceberg transported sediment. Darby and others (in progress) identify glacially rafted material from the western Arctic Ocean as having an abundance of forams, high sedimentation rate (1-2 cm/ky), and the presence of glacial erratics. (This material is referred to as a deglacial deposit in Table 1 from Darby and others (in progress)) which correlates foram abundance, sedimentation rate and the presence of IRD to glacial, deglacial and interglacial stages. In addition, the ice regime responsible for sedimentation is indicated. This approach partially depends on observing the sediment within the context of a core and therefore may not prove useful for determining the source of present sea floor sediment.

Evidence	***Glacial***	***Deglacial***	***Interglacial***
foram abundance	*low <500/g*	*high >2,000/g*	*high >2,000/g*
sedimentation rate	*low <.5cm/ky*	*high >1-2cm/ky*	*high >1-2cm/ky*
IRD (coarse sediment)	*low (variable)*	***high-10% IRD***	*low to moderate*
ice regime	*thick ice cover*	*thin ice cover* *many icebergs*	*thin ice cover* *few icebergs* *sea ice dominates*

Table 1. From Darby et al., in progress

Previous work by Clark and others also supports Darby and others' observations that icebergs transport a full range of poorly sorted sediments from boulders to silt while sea ice transports mainly clay and fine silt material (Clark et al., 1980).

b) Sea-Ice-Rafted Debris

Although some work has focused on texturally identifying sea-ice transported sediment, at present there are no accepted discriminating characteristics for it. Previous work determined that sea ice contains mainly fine grained material. Reimnitz and others (in progress) concluded that the sediment entrained by sea ice from the Beaufort sea is much finer than the source material on the shelf. In fact, they write, clays and silt are preferentially entrained by frazil during freezing storm events (Reimnitz et al., in progress). Figure 2 displays the percentages of sand, silt and clay for both shelf- and sea ice samples. The ternary diagram shows that sea floor samples landward of the 30 meter isobath thought to be principal source areas for entrainment into sea ice are generally coarser than SIRD. Reimnitz and others also noted that isolated samples contain large amounts of sand which they propose is a result of anchor ice formation during a severe storm at the time of fall freeze up. Therefore, grain size alone, as has previously been done, can not be used as the sole criterion for distinguishing sea-ice-rafted sediment from iceberg-rafted material.

c) Technique

Previous work using shape analysis: Dowdeswell (1982) used grain shape as a criterion for distinguishing basal from englacial grains. He determined that englacial grains are more angular and rough than the basal grains. These results were thought to help clarify the debris transport path through a glacier.

Dowdeswell and Dowdeswell (1989) studied the character of debris from Spitsbergen icebergs. Among other characteristics they found systematic differences in clast shape. They concluded that clasts of sub-rounded shape are likely to be basally derived, whereas those of

supraglacial origin are from rockfall onto the parent glacial surface and tend to be more angular. They suggest that the occurrence of angular clasts in the glaci-marine sedimentary record implies the presence of nunataks or valley walls, rather than unbroken ice sheet surfaces.

Riester and others (1982) used grain shape to distinguish sands of a littoral zone, an inner shelf, and a mid and outer shelf. The basis of the distinction is the relative proportion of abraded versus irregular grains within each zone. They found that the inner shelf zone contained significantly more irregularly shaped grains than the outer zone, which had more abraded grains.

Previous work using surface features:

In a similar study Krinsley and Donahue (1968) used surface textures of quartz sand grains to interpret environment of transportation and deposition. They found the method useful for distinguishing between littoral, aeolian, glacial, diagenetic and a combination of these four environments.

Hill and Nadeau (1984) used quartz-grain surface textures to interpret the transport history of sands from Beaufort Sea drillcores. They were able to distinguish grains which had undergone glacial processes, subaqueous transport and aeolian transport based on the surface features.

Study Area and Samples

The SIRD samples with the prefix AOS-94 were collected by Reimnitz of the USGS from the Beaufort Sea which is located at the southern end of the Canada Basin between the Chukchi Sea and the Canadian Archipelago. They were collected during the 1994 Polar Star cruise from across the North Pole. (Figure 3 shows the sample locations and Table 2 lists the coordinates). The samples were collected by scraping sediment from the surface of ice floes.

The glacial samples which were provided by Larry Phillips of the USGS are from two high resolution piston cores, PC-26 and PC-27, from the East flank of the Northwind Ridge (NWR). The Northwind Ridge is a high standing continental fragment surrounded by oceanic crust which is

isolated from fluvial or turbidite depositional systems. The samples are strongly oxidized, bioturbated pebbly sandy mud (Phillips et al., in progress). Complete core descriptions are found in Phillips and others (in progress).

For the purpose of this report glacially derived sediment or iceberg transported sediment refers to material that has been deposited by icebergs, but does not necessarily not refer to sediment that was deposited during a glacial period. Figure 4 shows the correlation between climate and sedimentation process.

Methods

Grain Size Analysis

Analysis of particle size can reveal much about the origin and dynamic conditions under which a sample was transported and deposited. Sediment textural characteristics were determined using a combination of sieving and pipetting. The coarse fraction was analyzed by sieving while the fine fractions were determined by pipetting. Sieving was the chosen method as opposed to a settling tube to avoid loosing the sand fraction needed for other analyses. In order to compare these data to previous data pipetting was used.

The analysis ideally requires approximately 10 grams of sediment. When ten grams were not available, smaller samples were used. To separate the coarse from the fine fraction the samples were wet sieved with distilled water through a 0.063 mm screen. The sand fraction was then resieved at 1.0 phi intervals after which it was dried and weighed to the nearest .001 gram to determine the sand sizes. Due to the method chosen and small sand percentages the data are reported in 1.0 phi intervals. There was not enough sand in many of the samples to measure smaller phi intervals.

To eliminate organic matter, the remaining mud was oxidized by soaking the sample in 5 ml. of 30% hydrogen peroxide and 200 ml. of distilled water overnight, after which the sample was lightly boiled for 2-3 hours to remove the excess hydrogen peroxide. Soluble salts were

removed by centrifuging and decanting water from the sample. In order to disperse the clay, Calgon (sodium hexametaphosphate) was added, whose weight was later subtracted. Pipette withdrawals were made using withdrawal times and depths from Carver (1971). The silt-and clay fractions are reported in 1.0 phi intervals down to 14 phi. For textural comparison the results were processed through a statistical package (USGS textural analysis program SDSZ) to determine mean size, sorting and skewness according to Folk and Ward (1957).

Surface Features and Grain Shape

Investigating the combination of surface features and/or grain shape of sand grains is often used to distinguish between various depositional environments and processes which helps to reconstruct a particle's physical and chemical history.

The term shape is a complex idea with many different interpretations. The terminology used in this thesis is based upon Barrett (1980) and Boggs (1987) who state that particle shape is composed of three aspects: form, roundness and surface texture. *Form* is most significant to a grain's morphology referring to its gross or overall shape reflecting variations in geometric proportions. Form is usually quantified as sphericity, elongation, or flatness. *Roundness (angularity)* is superimposed on form and reflects the shape of the corners. *Surface texture* reflects variations of the particle surface between the corners and is superimposed on the corners. The research undertaken in this thesis compares the form of sea ice rafted debris to that of iceberg rafted debris by the use of grain shape analysis, while the SEM analyzes the surface feature aspects of the grains. Both the SEM and image analyzer provided roundness/angularity data.

Analyses of grain shape and surface features were done using only quartz grains for two reasons. First and foremost, quartz is the most abundant mineral grain in the sea ice samples which do not contain significant sand. Secondly, past studies have shown that quartz due to its crystallography preserves surface features.

Surface Features

The quartz grains' surface features were observed under an SEM. Krinsley and Doornkamp's *Atlas of quartz sand surface textures* (1973) served as a guide for observing and interpreting the surface features.

The 180-300μm fraction was viewed under the SEM because grains much finer than 200μm are predominantly composed of flat cleavage faces (Krinsley and Doornkamp, 1973) and lack diagnostic features. To isolate the 180-300μ fraction the samples were wet sieved then picked for quartz under a binocular microscope. Although 15 grains are thought to give a valid statistical representation of the sample (Krinsley and Doornkamp, 1973), 20 grains from each sample were randomly selected for observation. The grains were boiled in a hydrochloric acid solution for 20 minutes to remove any adhering fine particles and/or calcium carbonate, then washed in distilled water to remove the acid. The grains were air dried and placed on a stub with double stick tape and coated with 75 nannometers of gold-palladium in a sputter coater and analyzed with a Philips XL40 SEM. An x-ray attachment was used to determine the elemental composition and verify that a quartz grain was selected.

Every grain was photographed and each surface feature was logged as absent, present, common, or abundant. "Absent" was used for features which cover <2% of the grain. "Present" means that the feature covers 2-25% of the grain's surface. Common indicates that 25-75% of the grain exhibits that feature and "abundant" refers to a feature which blankets >75% of the grain. In order to quantitatively compare the two types of sediment, the results of the SEM analysis were translated into a numerical system from zero to 3 (absent to abundant). The numerical values were then averaged to determine how common the surface feature is. The SEM images all contain scale bars which represent 100 microns unless otherwise written on the photograph.

Roundness/angularity and Relief

In addition to surface features, the relief and roundness/angularity of grains were observed under the SEM. The relief was visually determined to be high, medium or low which was also given a numerical value of 1, 2 and 3 respectively. The grain shape is described as angular, sub-angular, sub-round and round numerically represented by 1, 2, 3, and 4 (4 representing round grains). This scheme was modified from one used by Margolis and Krinsley (1974).

Grain Shape

The challenge of comparing grain shapes in a more detailed and less subjective way than describing them as round or angular has benefited from recent advances in image analysis. Grain shape analysis is based on the idea that a particle's shape can be represented by a two dimensional outline. The outline is a closed curve, and when "unrolled" is actually a curve of a periodic function. Fourier analysis is a mathematical way to describe a particle's shape by a matching Fourier series. With Fourier shape data a discriminant function analysis determines if the two sample types have significantly different shapes.

Since the shape of sedimentary particles is, to some degree, a function of composition and size (Kennedy and Ehrlich, 1985) measurements were restricted to 180-300 micron grains to minimize the effects of grain-size variations upon grain shape. Two hundred fine to medium sand grains from each samples were mounted on a microscope slide with glycerin, which was then heated to permanently attach the grains to the slide. The outlines of grains were digitized using an automated image analyzer (AIA), which is a microscope equipped with a video scanner as well as a computer for quantifying the grain shape (see Figure 5 for a schematic diagram of the equipment used). In this process a black and white camera projects a two dimensional image of the grain from a standard binocular microscope to a video screen. The ART3 program digitizes the edges of the quartz grains so that they can be quantifiably compared using a closed form Fourier analysis by the program CFOURIER. The image of the grain appears dark since the grain is lighted from

below. The outline of the grain is sharpened on the screen using the microscope focus knob and brightness and contrast features so that the computer can scan the pixels of the video image and record the boundary points as x, y coordinates. As the coordinates are being computed the centroid of the grain is being determined. The next step is to prepare the data for the Fourier transform analysis by converting the x, y coordinates into polar coordinates (radius versus angle). The radius is the distance from a boundary point to the centroid; the angle is measured between the horizontal line bisecting the centroid and the boundary point. The 2-dimensional shape of the grain is quantitatively described by the use of a Fourier series in closed form, which uses a summation of cosine wave to characterize the boundary of a grain. The Fourier series breaks down the grain outline into "n" components of shape called "harmonics" and measures the relative contribution or amplitude of each of these components to the grain's shape.

The Fourier series as developed by Ehrlich and Weinberg (1970) is

$$\mathbf{R(Q)} = \mathbf{R_0} + \sum_{n-1}^{\infty} Rn \cos(n\mathbf{Q} - \mathbf{Fn})$$

where

RQ = function representing the shape of the quartz grain

Q = the polar angle measured from a reference line

$\mathbf{R_0}$= the average radius of the particle

n = harmonic number, $1\text{-}\infty$

Rn = harmonic amplitude

Fn = harmonic phase angle

The shape of the quartz grain is represented by the function **R(Q)**, which is defined as the circle of radius $\mathbf{R_0}$ to which is added a series of cosine curves (harmonics) of various amplitudes Rn, and phase angles (**Fn**). n is the harmonic number.

The lower harmonics describe gross form, for example elongation, and increasingly fine scale shape components are represented as higher orders. In general, the *n*th harmonic represents the shape of an *n*-leaved clover (Dowdeswell, 1982). Figure 6 shows graphic representation of the 2-24 harmonics. The result was a voluminous data set including 24 harmonics for 200 grains for each sample. To reduce and analyze the data a discriminant function analysis (DFA) was run using the program STATISTICA to determine if the two sample types are distinguishable by shape and if so which of the 24 harmonics distinguish them. The DFA attempts to classify the grains into one of the two ice transport mechanisms based on the harmonic amplitude data. Mathematically, DFA computes a transform a forward stepwise discriminant analysis to build a model for separating the two types of grains. Based on the model from the discriminant function analysis new grains (not included in the model) were tested to determine to which group (SIRD versus IRD) they belonged. The model predicted classification based upon their shape. This last step assesses the reliability of the model. In addition, the statistical significance of the model was tested. Figure 7 shows the analytical procedure for the shape analysis.

Grain Size Analysis

Grain Size Data

IRD

Table 3 summarizes IRD gravel, sand, silt, and clay percentages as well as statistical data such as median size, mean size, sorting coefficient, skewness and kurtosis (after Folk and Ward, 1957). IRD contains from 1 to 11% gravel averaging 4% by weight. The sand and silt percentages are similar averaging 23 and 29%, respectively. Clay-sized particles compose the remaining 45% of the sample. The sand % ranges from 16 to 26%, silt ranges more widely from 6-39%, while ranges from 27 to 68%.

IRD samples have a mean size of 7.13 phi (very-fine silt) while the median size is 7.63 phi (also very-fine silt) showing a phi skewness coefficient of -0.23. The distribution is skewed

towards the smaller values (coarser-grain sizes). This is due to the "tail" of gravel in the samples (Fig. 8). The sorting coefficients for these samples range from 2.88 (very-poorly sorted) to 4.53 (extremely-poorly sorted) averaging 3.92 (very-poorly sorted) (Table 3 and 4).

The kurtosis coefficient, which is a ratio of the sorting in the extremes of the distribution compared with the sorting in the central part, for glacial samples ranges from 0.51 to 1.00 and averages 0.8 meaning the samples are platykurtic. This indicates that the tails are better sorted than the central portion, but not significantly so. The sorting is basically equally poor throughout the sample.

The 1.0 phi interval histogram (Fig. 8) has an uneven distribution, showing bimodal nature of glacial sediment: one mode at the sand silt boundary (4 phi) and another in the clay range as well as a coarse tail extending through -3 phi (gravel).

SIRD

SIRD samples differ most notably from IRD in lacking gravel and in having very little sand. Clay-sized particles dominate. The 1.0 phi histogram (Fig. 9) shows the overall trend of increasing weight percent as the grain size decreases. When averaged the samples contain 5% sand, 33% silt and 62% clay (Table 5 and 6). Thirty nine percent of the clay is in the 10-14 phi range. The sand % ranges from 0 to 32%, while the silt and clay percentages vary more widely from 12 to 68% and 31 to 85% respectively. The 5% average sand figure may be misleadingly high due to the high sand content of samples 215-E3 and 226-1 which have 32 and 29% sand. Distinct entrainment processes (discussed elsewhere) may account for these high values. If these samples were removed from the group of SIRD samples, then the average sand percent decreases to 2% which I feel more accurately describes SIRD. This figure is more consistent with previous grain-size analyses of SIRD which determined sand to be a small component (Kempema et al., 1989; Nürnberg et al., 1994).

The mean grain size for these samples ranges from 6.60 to 11.67 phi averaging 9.02 phi (clay) which is close to the median size of 9.01 phi. The average phi skewness of 0.00 indicates that grain size distribution is nearly symmetrical about the median diameter. (The mean size equals the median size.) The sorting coefficients for this suite of samples vary minimally from 2.22 to 3.79 averaging 2.85 (very poorly sorted), although not as poorly sorted as the glacial samples.

The kurtosis coefficient, the ratio of the sorting in the extremes of the distribution compared with the sorting in the central part for sea ice samples is 0.89 which means the samples are mesokurtic. This indicates that the tails are better sorted than the central portion, but insignificantly so.

There are two strong modes in this sample group (Fig. 9): one in the medium to coarse clay range (8-10 phi) and a second in the coarse silt range(4-5 phi).

Discussion of Grain Size Data

The ternary diagram (Fig. 10) shows the gravel/sand, silt and clay ratios for the two sample types. IRD samples are the only ones that contain any gravel. Furthermore, icebergs transport six times more sand than sea ice samples do. The diagram illustrates that the IRD samples are coarser than SIRD samples with average mean sizes of 7.13 and 9.02 phi, respectively. The combined gravel and sand % is 27% for the IRD as compared to only 5% sand for the SIRD samples, which are composed primarily of clay material. The entrainment mechanisms for sea ice and glaciers help explain this difference in grain size characteristics. As glaciers move from continental areas to the sea they pick up material along the bottom, sides, and top of the glacier. The glacier is capable of entraining large particles, even boulders which may eventually get deposited in the ocean. On the other hand, the entrainment mechanism for sea ice involves significantly less energy because, as the scavenging ice particles float toward the surface they pluck sediment from the water column. This process generally can not pick up large gravel size sediment. Although the formation of anchor ice can entrain larger particles or even large percentages of sand into sea ice (such as in

samples AOS 215-E3 and AOS 226-1) scavenging by frazil is the dominant process of ice formation, which explains why SIRD is generally fine grained.

The gravel/sand/silt/clay bar graphs (Figs. 11 and 12) shows that clay dominates SIRD samples while IRD samples have a more even distribution of sediment sizes. In terms of sorting, both sample types are very poorly sorted, but IRD samples are even more poorly sorted (coefficient 3.92) as opposed to SIRD (2.85). Once again, the entrainment process may account for the difference in sorting coefficients. A glacier collects and transports material randomly, while sea ice selects the finer particles to incorporate into the ice canopy of the Arctic Ocean due to one of three reasons: a) The only particles available for scavenging on the sea floor or in the water column are the finer ones, b) the process can not transport the available coarser sediment, or c) due to the long life of an iceberg and its steep topography the fines may have been lost during its drift. Grain size analysis of sea-floor surface sediment (Table 7) (Figure 13) indicate that they do contain coarser material than what is entrained into the sea ice. The sea floor samples selected for this grain size analysis represent fallout from sea ice and the water column and should not contain turbidite deposits since they were taken from ridges. This supports the idea that the entrainment process is selective rather than the scarcity of larger particles on the sea floor, and explains the difference in sorting between IRD and SIRD.

Conclusions Based on Grain Size Study

Icebergs deposit generally coarser and more poorly sorted material than sea ice, but the data did not show definitive grain size determinants for the two sediment types. Many researchers have used the presence of gravel size material (glacial erratics) to indicate glacial deposits. The data would support this assessment since I did not find any gravel in the sea ice samples. Besides the presence/absence of gravel I conclude that it is misleading to use grain size as a distinguishing factor since both types of ice carry the range of grain sizes from sand to clay. Furthermore, other studies have found gravel in SIRD, which may be explained by the formation

of anchor ice. It is true that the relative percents of the coarser material can suggest iceberg rafted material, but the overlap in grain size makes this distinction weak at best. The average grain size, sorting, skewness, or kurtosis are not distinct enough to be used as distinguishing features.

Grain Shape Analysis

Grain Shape Data

IRD and SIRD

Results of shape analysis conclude that SIRD and IRD are not distinguishable by shape. The computer-generated model of IRD versus SIRD grain shapes did not successfully classify grains of supposed "unknown" origin. After harmonic data were gathered, a discriminant function analysis was run, which attempted to classify the grains into one of the two mutually exclusive groups based on amplitude values. The results of that analysis are presented in Table 8 which shows that the program correctly classified 685 sea ice grains out of a total 1220 (or 56%). When "unknowns" of glacial origin were put through the classification process the model once again correctly assigned only 56% of the grains. This is little better than a random assignment for two grain types. Therefore, the data suggest that the shape analysis as was performed in this research is not a viable method for differentiating between SIRD and IRD. However, there are a few minor differences in the grain shapes worth noting.

Discussion of Grain Shape Data

Table 9 shows the maximum, minimum and average harmonic amplitudes for harmonics 2-24 for both sediment types. In general harmonic amplitude decrease as the harmonic number increases. The graphs of these data (Fig. 14) show that sea ice grains have characteristically higher average harmonic amplitudes for the lower harmonics (#2-17, except for harmonic #14). In particular, sea ice has much higher harmonic amplitudes for harmonic #2-7. The converse of this is true for most of the higher harmonics. Glacial sediment has higher harmonic amplitudes for

#19, 22, 23 and 24 (Fig. 15). The sea ice average harmonic amplitude for #18 and 20 equal those of glacial sediment. This trend suggests that irregularly shaped features contribute more to the overall shape of the glacial grains than to that of the sea ice grains. The sea ice grains lack these fine scale irregularities in the grain outlines, which may be the result of chemical etching which serves to smooth the grain surface and obliterate any relict surface irregularities. Abrasion encountered during transport and deposition may have erased small-scale irregularities. This may be evidence that sea ice sediment was in a high energy zone with increased abrasion while in the entrainment zone of less than 30 meters water depth. The increased higher amplitudes for the glacial grains indicate that they may have undergone a transport process that formed shape irregularities such as the grinding associated with glacial transport. The shear stress created by glacial transport may have caused the formation of jagged grain outlines.

Table 9 also shows that in all but the 22nd and 23rd harmonics sea ice amplitudes vary more widely than does glacial sediment. This comparison suggests that the shape of sea ice sediment varies more than does that of glacial sediment. This wide variation in the sea ice grain shape may be responsible for the lack of success with this method. The glacial grains may have a distinct shape, but when compared with the wide variety of sea ice grains, they are not distinguishable.

The harmonics most often used in shape studies are 2 and 19 or 20 (Kennedy and Ehrlich, 1985). The mean amplitudes of harmonic 2 are viewed as approximation of elongation or sphericity (Cai, 1994). A grain with a high harmonic 2 amplitude is more elongate or less spherical than a grain with a low second harmonic amplitude. The second harmonic (Table 9 and Fig. 14) shows the most significant difference between sea ice grains and glacial grains with average harmonic amplitudes of 0.217661 and 0.210893 respectively. This difference means that the second harmonic shape contributes more to sea ice grains than to glacial grains, which implies that sea ice grains are more elongate and that glacial grains are more spherical. Once again, this

distinction is not powerful enough to distinguish the grains, but suggests that there are minor shape differences.

The other commonly used harmonic is the 19th or 20th, which is a measure of roundness or angularity. A grain with a high 19th harmonic amplitude is more angular and less round than a grain with a lower 19th harmonic (Cai, 1994). Glacial sediment has a higher 19th harmonic than does sea ice sediment (0.0037 versus 0.0035 respectively) (Fig. 15) suggesting that IRD is more angular and SIRD is more rounded. This fact corresponds to visual SEM observations which show IRD to be more angular than SIRD.

To further verify that the two sediment types can not be distinguished by shape data alone, the harmonics with the largest differences (#2 and #3) between the averages were plotted as a scatter graph. The results (Fig. 16a and b) show that SIRD and IRD fall into the same field, without any possibility of spatial separation. Therefore, even the harmonics with the greatest differences can not successfully distinguish them.

Conclusions Based on Grain Shape Study

This research shows shape analysis to be inconclusive in distinguishing SIRD from IRD based on shape alone. The lack of success of this part of the study may be due to the underlying assumption that a detrital quartz grain will have surface features or shape that are related to processes that have operated upon it during entrainment and transport (Mazzullo and Magenheimer, 1987). This assumption may not be valid for ice entrainment and deposition. It is possible that quartz grains from a given source have a shape that reflects the genesis or lithology of the source and are distinct from the shapes of quartz grains from other sources (Mazzullo and Magenheimer, 1987). Therefore, the ice transport mechanism would be irrelevant to the particle's shape. If this is the case then no method of shape analysis will yield successful results.

On the other hand, the lack of success with this shape analysis may lie in the methodology. The method used in this research may not be sensitive enough to detect the small scale shape

differences. For example, the digital outline of the grain may not be an accurate representation of the particle's shape since the outline is limited by the pixel resolution. The digitized grain outline is composed of pixels on the screen which may not correspond precisely to the grain outline. The detail lost in the digitization process could be the subtle differences in the grain shape that we are trying to detect. Furthermore, 24 harmonics may not be detailed enough to show small scale shape irregularities that 96 or even 48 harmonic could detect. This does not indicate that there were no shape differences; on the contrary, when the SEM and shape data are viewed together they hint towards a similar conclusion, which is that there are differences in shape and surface features. The SEM and 19th harmonic data suggested that glacial grains are more angular than sea ice material. Therefore, I conclude that there is some indication that a more detailed shape analysis could yield conclusive results in distinguishing SIRD from IRD.

Surface Feature Analysis

Surface Feature Data

Arctic sedimentation processes may be reflected in microtextures of sand-size quartz grains. To evaluate this the observed surface features were divided into three groups and will be discussed as categories of features since the forces or processes that formed each group of features are related. The categories include features resulting from mechanical breakage, impacts, and chemical activity. The features observed on the grains included the following mechanical breakage features: Small breakage blocks (<1 micron), large breakage blocks (> 1 micron), small conchoidal fractures (<1 micron), large conchoidal fractures (>1 micron), fractured surfaces, parallel and sub-parallel step like fractures, arc step like fractures, broken cleavage plates, and relief. The following impact features were observed: Dish-shaped concavities, angularity/roundness, mechanical v-shaped impact pits, abraded surfaces , upturned plates, and straight or curved scratches (grooves). The following chemical features were observed: Oriented

v-shaped etching, irregular pitted surfaces due to silica dissolution, silica precipitation, and etching pits.

Description and interpretation of surface features from Krinsley and Doornkamp, 1973 and Margolis and Krinsley, 1974.

Mechanical breakage features: *Breakage blocks, conchoidal fractures, and fractured surfaces* result from physical stress on the grains. *Parallel and sub-parallel step like fractures* are the result of shear stress on quartz grains. *Arc step like fractures* represent percussion fractures (sub-variety of conchoidal fractures). *High Relief* suggests that the grain has been in a high energy environment and undergone mechanical breakage. *Angularity* is a grain characteristic which refers to the shape of the corners. Angular edges are often the result of extreme shear stresses especially in a high energy environment.

Impact features: *Dish-shaped concavities* , often found on aeolian grains, result from grain to grain impacts while the grain is rolling and saltating, especially when the contact is in the form of uniform compressional stress. This feature is often used to distinguish aeolian grains from other types of sands. *Rounded edges* often result from subaqueous abrasive action or aeolian transport (grain to grain impacts). *Mechanical v-shaped impact pits* are notches cut into the tops of cleavage plates which are often thought to be a result of subaqueous abrasive action. *Upturned plates* are the result of abrasive activity. Upturned plates are traces of a secondary cleavage direction. They consist of a series of parallel plates with depressions between them or parallel lines slightly raised above the dominant cleavage surface, which often occurs on aeolian grains due to wind produced grain impacts. Upturned plates are produced on the fractured portions. *Abraded surfaces* are the result of abrasive activity often in a high energy subaqueous environment. The surface will show evidence of many grain to grain impacts resulting in a pitted look, which is unlike chemical etching in that the pits are randomly oriented. *Straight or curved scratches (grooves)* are the result of grain-to-grain impact in a high energy subaqueous environment. They are produced by two grains

sliding past each other removing fine splinters from the surface of the grains. This surface feature results when there is not enough energy to produce mechanical v's or dish-shaped concavities.

Chemical features: *Oriented v-shaped etchings* are crystallographically oriented etching pits. They often occur along planes of weakness and are the result of long exposure to marine conditions often in a low energy environment. *Irregular pitted surfaces* which look like the grain is peeling or wearing away is due to silica dissolution in a subaqueous silica deficient environment. *Silica precipitation* appears as bulbous growths on the grain and subdues grain angularity and obliterates relict surface features. This type of alteration occurs mainly in a subaqueous environment where there is excess silica in solution. *Etching pits* (solution pits) circular or subcircular holes often have silica precipitation on the rims. Table 10 summarizes the energy level, environment and processes involved in creating each surface feature.

SIRD Surface Features

General Description

Detailed observations for each grain are presented in appendix 1 and the results of the SEM analysis are summarized in Table 11, where the numerical scores for all the grains within a sample are averaged to facilitate comparison of grain types. SIRD grains are generally subrounded to rounded with minimal relief, and have been extensively altered by chemical rather than mechanical processes. Chemical alteration features, such as crystallographically oriented etching pits, irregularly pitted surfaces, signs of silica precipitation and dissolution are significant and in many cases cover over 75% of the grain's surface. One of the most common microfeatures is the rolling topography created by silica precipitation within the valleys produced by upturned plates. The result is a hummocky surface. Another dominant chemical feature is the irregularly pitted surface due to silica dissolution. Less common but striking are the deep etching pits also created by silica dissolution. These grains show few relict features since they have probably been subdued or

obliterated by intense chemical alteration. However, the most striking aspect of SIRD is the lack of significant mechanical breakage features.

Surface Feature Data

Relief and roundness: SIRD samples have low relief with a relief value 2.8. 94% of the sea ice grains have a relief value of 2 or 3. This feature is consistent throughout the samples, except that 2 of the grains have a relief value of 1. The roundness data for these grains averages 3.4 which represents a sub-rounded to rounded grain outline. Ninety-three percent of the grains observed have a roundness value of 3 or 4. Plate 1 shows four typical sea ice grains.

Mechanical Breakage Features: The following features scored less than 1 when averaged, meaning these features covered less than 2% of the grains: small and large breakage blocks, small and large conchoidal fractures, parallel and sub-parallel step like fractures, arc step-like fractures, straight and curved scratches, and broken cleavage plates. The lack of these mechanical features, in part, account for SIRD's overall roundness and lack of relief.

Impact Features: Although there was little evidence of mechanical breakage features, signs of grain-to-grain impacts were evident. Of the four impact features mentioned two were seen. These microtextures include upturned plates and impact pits. Impact pits score an average of 1.2 which means they are "present", while upturned plates scored 2.0, which means they are "common". The impact pits are v-shaped depressions randomly oriented and provide a pitted, "banged up" look to the grains (Plate 2). The grain surface has small nicks in the shape of a "v". The upturned plates, which occur primarily on the edges of grains, were seen as cleavages traces that have been filled in with silica precipitation. The result is a rolling topography on the grain surface. Plate 3, photo A shows a grain with upturned plates between which silica has precipitated. Photo B shows a close-up of that feature. The other two impact features, dish-shaped concavities and an abraded surface, were not present on the grains. There are a few possible explanations as to why the last two impact features were not observed on the grains.

According to Margolis and Krinsley (1974) grains smaller than 500 microns do not show signs of rolling and saltation, or the impacts on these grains were strong enough to produce upturned plates and mechanical v's but not strong enough to produce dish-shaped concavities or any abraded surfaces. Possibly the grains were in a medium-energy environment.

Chemical Features: Chemically produced surface features dominate SIRD grains. The appearance of a grain is a result of the following four features combined: Oriented v's, etching pits, irregular pitted surface due to silica dissolution and silica precipitation. These features scored an average of 1.0, 1.8, 2.2 and 2.5 respectively. Etching pits are circular holes that dip into the surface of the grain. Plate 3C and D show deep etches caused by chemical breakdown. The grain in Plate 3C shows silica precipitation on the rim of the pit, while the pit in 3D shows silica precipitation in the interior of the pit. Another common feature of sea ice grains is an irregularly pitted surface caused by silica dissolution, which gives the grain an uneven scaly appearance. It looks as if the grain's surface is peeling off. Plate 4 shows a grain that has undergone intense chemical alteration. Photograph D shows the chemical breakdown of the outer surface of the grain. Plate 5 shows examples of oriented v-shaped etching common to sea ice grains. Note how aligned the chemical features are compared to the mechanically produced impact pits of Plate 2. These features are mainly found on the ends of the grains that have been most exposed to weathering processes. Of all the observed features on SIRD, silica precipitation has the most significant effect on the overall appearance of the grain's surface for a variety of reasons:

a) It softens or obliterates any relict structures such as breakage features.

b) The precipitate is often deposited in topographically low areas on the grain which serves to smooth out a grain's outline making it appear more round. This is especially common in the cavities between the upturned plates.

IRD Surface Features

General Description

Fresh quartz grains from a glacial environment are more angular with jagged sharp edges and higher relief than grains carried by sea ice. Mechanical breakage features dominate the surface including breakage blocks, conchoidal fractures, parallel and sub-parallel step fractures, arc-shaped step fractures, and broken cleavage plates (Plate 6). The conchoidal fractures vary in abundance and size; some individual fractures are <1 micron while others cover an entire 300 micron grain. They are irregularly distributed across a grain and appear to be randomly oriented. Fresh fracture surfaces are very smooth due to lack of solution and precipitation. When compared to SIRD, chemical alteration is of less significance on these grain surfaces. Grain to grain impact features are of minor to moderate importance. Once again impact pits and upturned plates are observed, while dish-shaped concavities and abraded surfaces are not. The lack of chemical and impact features may be the result of the "freshness" of the glacial grains, which have not been subjected to the environments or conditions that produced these features. Their glacial past is too recent for them to have experienced subaqueous conditions producing chemical alteration, or high energy environment that could produce impact features.

Surface Feature Data

Relief and roundness: IRD grains have a high degree of relief averaging 1.7 (medium-high). Note the high relief of Plate 7 grain A. In addition, the grains are angular to sub-angular scoring 2.5 (Plate 6). The angularity and high relief of IRD result from glacial grinding which serves to produce fresh jagged surfaces which have not yet been subdued by chemical alteration or rounding of edges by grain to grain impacts. The severity of the angularity and relief depends on the relative "freshness" of glacial grains.

Mechanical Breakage Features: These are the main diagnostic features of glacial grains. The following breakage features all scored above 1 when averaged: large breakage blocks, small

and large conchoidal fractures, parallel and subparallel step fractures, arc-shaped step fractures, and broken cleavage plates. These scored 1.1, 1.2, 1.6, 1.6, 1.4, 1.2, and 1.1 respectively. Often a combination of these features covers the entire grain surface. Plate 7B shows a good example of parallel step fractures. Distinct conchoidal fractures are visible on Plate 7C. Arc step-like fractures dominate the fresh surface of Plate 7D. Once again, the grains are often too fresh for these features to have been modified by superimposed features such as chemical alteration or impact features.

Impact Features: Features such as impact pits and upturned plates were of moderate importance on IRD. When averaged they scored 1.0 and 1.5 respectively. The lack of significant impact features suggest that the grains had not been in a high energy environment that would have produced grain to grain impacts.

Chemical Features: The data suggest that chemical alteration is of moderate importance on these grains. Oriented v's were not present on the grains, however, evidence of irregular pitted surfaces, silica precipitation and etching pits were present. These features scored 1.5, 1.8 and 1.7 respectively.

Roundness/angularity: Figure 17 shows the frequency percentage of grains per sediment type that fall into each of the four categories of surface roughness from angular to rounded. Glacial grains are dominated by the angular categories: 80% of the grains are angular, and 85% of the grains are sub-angular . Sea ice sediment comprise 59% of the sub-rounded grains and 79% of the rounded grains.

Classification of Grains Based on Surface Features

Since few grains possessed all of the "IRD or SIRD features", a categorizing system was developed to represent the entire spectrum of grains. In this system the grains fall into four categories reflecting gradational changes, therefore, the assignment of a grain into one of the four types is somewhat subjective. The classification system attributes type I and II grains to glacial

transport, while type III and IV reflect sea ice transport. It should be noted that the grains were classified strictly on the basis of their surface features. The types are:

Grain type I: Fresh glacial grain (Plate 6)

Grain type II: Modified glacial grains (Plate 8)

Grain type III: Modified sea ice grains (Plate 9)

Grain type IV: Purely sea ice grains (Plate 1)

Grains of type I (Plate 6) have all of the distinctly glacial features mentioned above such as a high degree of relief, sharp angular outline, an abundance of breakage features and an absence of chemical features. The fracture surfaces are smooth and unaltered. Fractures cover 75-90% of the grains' surface. These grains are considered fresh glacial grains. 86% of the grains of this category were from a glacial source and 14% from sea ice (Table 12).

Type II and III represent grains with a combination of features. The features are not strictly glacial or sea ice, but have a mixture of the two types. In type II the glacial features dominate, while type III grains show more of the sea ice features. Type II grains (Plate 8) are similar to type I in overall appearance, but have been modified. Their angular outlines have been modified by impacts or chemical alteration. The grains are more round than type I but still have many glacial breakage features. Seventy-one percent of type II grains are considered to be of glacial origin, while the remaining 29% are from sea ice.

Type III grains (Plate 9) appear more similar to SIRD than IRD. The edges are better rounded because of increased silica precipitation which smoothes out the grains outline, and because of continued impacts which round the corners of the grains. Impact features are evident. These grains have lower relief than type I or II. Grains in this category do not show any of the distinct glacial features. The breakage features are beginning to diminish because of the silica precipitation covering them. At this point the relict features of the grain are no longer visible. According to the categorizing used here 86% of type III grains are SIRD, while the remaining 14% are IRD.

Grains of type IV have most of the sea ice characteristics such as roundness, lack relict features, show low relief, and an abundance of chemical alteration without any of the breakage features. 86% of grains assigned to this category are from sea ice grains and 14% from icebergs.

Type	Glacial	Sea Ice	Total
Type I (fresh glacial grains)	**6 (86%)**	1	7
Type II (modified glacial grains)	**17 (71%)**	7 (29%)	24
Type III (modified sea ice grains)	5 (25%)	**18 (75%)**	23
Type IV (pure sea ice grains)	1	**6 (86%)**	7
Total	29	32	61

(Table 12)

Interpretation of Surface Feature Data

IRD and SIRD quartz grains have surface features that reflect a past mode of transport and deposition. One or two features can not distinguish the different transport mechanisms, but the combination and abundance of groups of surface features can. The grains carried by sea ice are more round, have a lower degree of relief and are characterized by an abundance of chemical alteration features. This is a result of the environment in which the sediment has been transported. As the sediment is carried by an ice floe it is in a low energy environment where breakage features are not likely to develop. Furthermore, impact features are also likely to be absent since the grains are not being tossed around by wind and wave activity. However, the grains are subjected to the weathering capabilities of sea water. Prolonged exposure to the sea water can lead to the chemical alteration which is so prevalent on the sea ice grains. Most of the grains show both silica precipitation and dissolution which suggests that there was more than one period of chemical activity. In general, more silica precipitation was seen rather than dissolution indicating a net addition of silica to the sand grains. One caveat: it is difficult to attribute the chemical features

wholly to the sea ice environment since grains entrained into sea ice have been lying on the sea floor before they were scavenged by ice crystals. It is impossible to separate the effects of the two environments, especially since it is difficult to determine how long the grain has been exposed to both. Although the two environments are similar in terms of the geochemistry and would therefore produce similar chemical weathering effects on the quartz grains, the environments differ in terms of the energy levels. Grains lying on the continental shelf in less than 30m water depth, where these grains were entrained (Reimnitz et al., 1993) would be subjected to abrasive wave activity creating some of the impact features seen on type III grains. The grains on a ice floe would be in a lower energy environment and therefore, would not have impact features.

The origin of glacial features is more easily understood than the origin of sea ice features. As grains are transported by glaciers on land they are subjected to intense compression and shear stresses which create distinct breakage features. Furthermore, chemical features such as etching have not been observed on fresh glacial grains because this type of weathering at high latitudes may require more time than is available since the last glaciation, i.e. 15,000-20,000 years (Strass, 1978).

Twenty percent of the grains were classified as either type I or type IV grains which means they have distinct glacial or sea ice features. The remaining 80% of the grains show a more complex set of surface features making it more difficult to determine their transport mechanism. To correctly assign these grains to an ice transport mechanism one must look at the relative contribution of glacial to sea ice features. The classification system worked for 71% of type II grains and 75% of type III grains. The problematic part of this system was the 29% of SIRD that was classified type II (modified glacial grains) and the 25% of glacial grains that was classified as type III (modified sea ice grains). There are a few explanations for grains that seem to have characteristics of both transport and depositional processes:

a) This mixing of unexpected surface features suggest that these grains have undergone a complex depositional history. For example, sediment found in sea ice may be reworked glacially

derived sediment, with glacial features still prevalent. The processes of sea ice entrainment, transport and deposition has not yet obliterated the glacial features. When a grain shows evidence of both mechanical and chemical processes the more recent episode will be superimposed on the grain. Plate 10 A and C show reworked glacial grains. Grain A (280#1) has a conchoidal fracture on the bottom part, but also shows evidence of chemical alteration on the top of the grain. Grain D is a close up of grain C which shows the chemical precipitate alongside a distinct fracture surface.

b) Another possible scenario which would explain why some of the grains interpreted to be of glacial origin show characteristics of sea ice is that during the depositional regime which was interpreted to be at a time of deglaciation sea ice sedimentation was also active. This would introduce grains with sea ice surface features into the core section which was previously thought to represent only iceberg transported sediment. This mixing of sediment sources and transport mechanisms may account for some of the "glacial grains" which look like sea ice sand.

Conclusions Based on Surface Feature Study

The SEM comparison of IRD and SIRD surface features and shapes proved to be the most diagnostic part of this research. Data indicate that grains from a glacial environment are more angular with jagged sharp edges and have higher relief. Mechanical breakage features dominate the grain's surface including breakage blocks, conchoidal fractures, parallel and sub-parallel step fractures, arc-shaped step fractures, and broken cleavage plates. Grains entrained into sea ice are generally subrounded to rounded with minimal relief and have been extensively altered by chemical rather than mechanical processes. Chemical alteration such as crystallographically oriented v-shaped etching pits, irregularly pitted surface, signs of silica precipitation and dissolution are significant and often cover over 75% of the grain's surface. The presence of only one or two features can not pinpoint the ice transport mechanism, but the abundance of specific types of features apparently can reveal the transport and depositional history of the sediment.

Conclusions of Entire Study

The sedimentation and climate history of the Arctic region remains somewhat blurred by the lack of criteria for distinguishing sediment carried by sea ice. This comparison of sediment transported by icebergs with sediment carried by an overlying sea ice canopy reveals a potentially powerful method for distinguishing the two sediment types and therefore the two ice transport mechanisms. Identifying the Arctic ice-transport pattern has important climatic implications. The data of this study show that the two sediment types differ slightly in terms of grain size and shape, but have very different surface features. The grain-size analysis shows that icebergs transport and deposit generally coarser, more poorly sorted material than does sea ice. Grain shape analysis suggests that quartz grains entrained into sea ice tend toward a more elongate form with rounded edges, while iceberg rafted grains have a more spherical form with angular edges. Although the size and shape analysis shows minor differences, neither is significant enough to reliably identify the ice transport mechanism. However, the analysis of surface features observed under an SEM suggests that the two sediment types can be differentiated by the abundance or absence of specific groups of surface features. The surface of glacial grains are dominated by mechanical breakage features such as high relief, breakage blocks, conchoidal fractures and step-fractures, while the surface of sea ice grains has an abundance of chemical features such as pits, evidence of silica dissolution and precipitation and oriented etching pits.

References

Barrett, P.J., 1980, The shape of rock particles, a critical review: Sedimentology, v. 27, p. 291-303.

Boggs, S.J., 1987, Principles of sedimentology and stratigraphy: Columbus, OH, Merriall Publishing Company, A Bell and Howell Company, 784 p.

Cai, J., 1994, Sediment yields, lithofacies architecture and mudrock characteristics in glacimarine environments [Dissertation thesis]: Dekalb, Northern Illinois University.

Carver, R.E., 1971, Procedures in Sedimentary Petrology, John Wiley and Sons Inc., 653 p.

Clark, D.L., 1990, Arctic Ocean ice cover; Geologic history and climatic significance, *in* Grantz, A., Johnson, L., and Sweeney, J.F., eds., The Arctic Ocean region, Volume L: Boulder, Colorado, Geological Society of America, p. 53-62.

Clark, D.L. and Morris, T.H., 1985, Arctic Ocean sediment texture and the Pleistocene climate cycle: Geological Society of America, 98th Annual Meeting, Orlando, Florida. Abstracts with Programs 17:7, p. 547.

Clark, D.L., Whitman, R.R., Morgan, K.A., and Mackey, S.D., 1980, Stratigraphy and glacial-marine sediments of the Amerasian Basin, central Arctic Ocean, p. 57.

Darby, D., Bischof, J.F., and Jones, G.A., in progress, Radiocarbon chronology of depositional regimes in the western Arctic Ocean: .

Dowdeswell, J.A., 1982, Scanning electron micrographs of quartz sand grains from cold environments examined using Fourier shape analysis: Journal of Sedimentary Petrology, v. 52, p. 1315-1323.

Dowdeswell, J.A., and Dowdeswell, E.K., 1989, Debris in icebergs and rates of glaci-marine sedimentation: observations from Spitsbergen and a simple model: Journal of Geology, v. 97, p. 221-231.

Ehrlich, R.., and Weinberg, B., 1970, An exact method for characterization of grain shape: Journal of Sedimentary Petrology, v. 40, p. 205-212.

Ehrlich, R., Brown, P.J., Yarus, J.M., and Przygocki, R., 1980, The origin of shape frequency distributions and the relationship between size and shape: Journal of Sedimentary Petrology, v. 50, p. 475-484.

Eppler, D.T., Ehrlich, R., Nummedal, D. and Schultz, P.H., 1983, Sources of shape variation in lunar impact craters; Fourier shape analysis: Geological Society Bulletin, v. 94;2, p. 274-291.

Folk, R.L. and Ward, W.C., 1957, Brazos river bar, a study in the significance of grain size parameters: Journal of Sedimentary Petrology, v. 27, p. 3-26.

Hill, P.R., and Nadeau, O.C., 1984, Grain-surface textures of Late Wisconsinan sands from the Canadian Beaufort shelf: Journal of Sedimentary Petrology, v. 54, p. 1349-1357.

Kempema, E., Reimnitz, E., and Barnes, P., 1989, Sea ice sediment entrainment and rafting in the Arctic: Journal of Sedimentary Petrology, v. 59, p. 308-317.

Kempema, E.W., Reimnitz, E., Clayton, J.R., and Payne, J.R., 1993, Interactions of frazil and anchor ice with sedimentary particles in a flume: Cold Regions Science and Technology, v. 21, p. 137-149.

Kennedy, S.K.., and Ehrlich, R., 1985, Origin of shape changes of sand and silt in a high-gradient stream system: Journal of Sedimentary Petrology, v. 55, p. 57-64.

Krinsley, D.H. and Doornkamp, J.C., 1973, Atlas of quartz sand surface textures: London, Cambridge University Press, 91 p.

Krinsley, D.H., 1980, Scanning electron microscope examination of quartz sand grain microtextures: Kwartalalnik Geologiczny, v. 24, p. 217-232.

Krinsley, D.H., and Donahue, J., 1968, Environmental interpretation of sand grain surface textures by electron microscopy: Geological Society of American Bulletin, v. 79, p. 743-748.

Margolis, S.V., and Krinsley, D.H., 1974, Process of formation and environmental occurrence of microfeatures on detrital quartz grains: American Journal of Science, v. 274, p. 449-464.

Mazzullo, J., and Magenheimer, S., 1987, The original shapes of quartz sand grains: Journal of Sedimentary Petrology, v. 57, p. 479-487.

Nürnberg, D., Wollenburg, I., Dethleff, D., Eiken, H., Kassens, H., Letzig, T., Reimnitz, E., and Thiede, J., 1994, Sediments in Arctic sea ice: implications for entrainment, transport and release: Marine Geology, v. 119, p. 185-214.

Phillips, R.L., Grantz, A. and McLaughlin, M., in progress, Summary of lithostratigraphy and stratigraphic correlations in piston cores from the Northwind Ridge, Arctic Ocean, from the USCG Polar Star, 1992: U.S. Geological Survey Open File Report 97-522.

Reimnitz, E., Barnes, P.W., and Weber, W.S., 1993, Particulate matter in pack ice of the Beaufort Gyre: Journal of Glaciology, v. 39, p. 186-198.

Reimnitz, E., Marincovich, L., McCormick, M., and Briggs, W.M., 1992, Suspension freezing of bottom sediment and biota in the Northwest Passage and implications for Arctic Ocean sedimentation: Canadian Journal of Earth Sciences, v. 29, p. 693-703.

Riester, D., Shipp, C.R., and Ehrlich, R., 1982, Patterns of quartz sand shape variation, Long Island littoral and shelf: Journal of Sedimentary Petrology, v. 52, p. 1307-1314.

Strass, I.F., 1978, Microtextures of quartz sand grains in coastal and shelf sediments, More, Western Norway: Marine Geology, v. 28, p. 107-134.

Thiede, J., Clark, D., and Herman, Y., 1990, Late Mesozoic and Cenozoic paleoceanography of the northern polar oceans, *in* Grantz, A., Johnson, L., and Sweeny, J.F., eds., The Arctic Ocean region, Volume L: Boulder, Colorado, Geological Society of America, p. 427-458.

Figure 1: Photo of anchor ice adhering to substrate

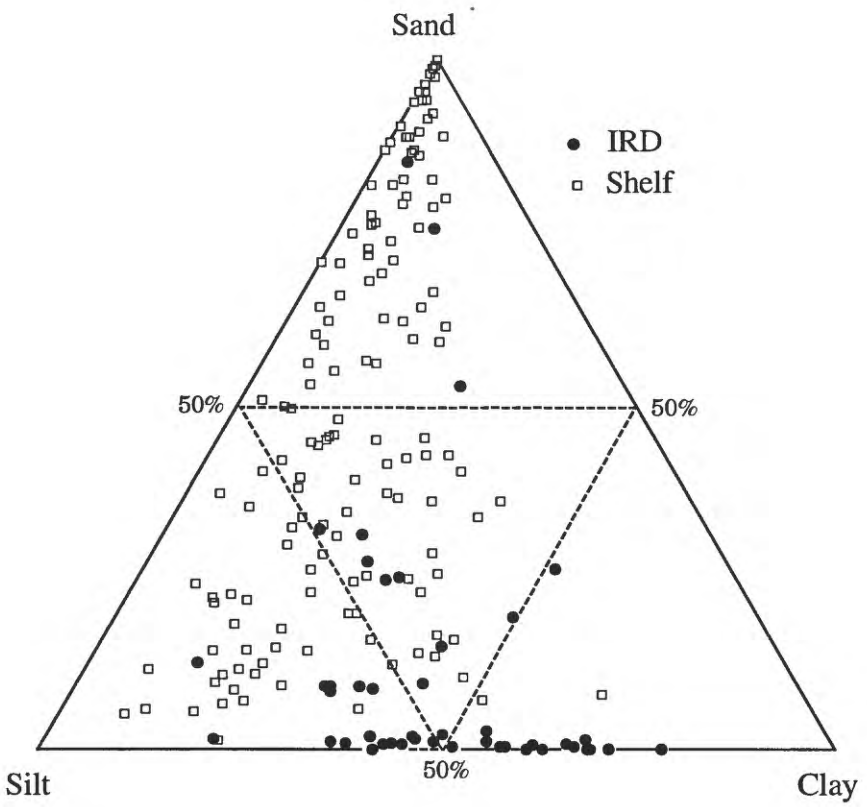

Figure 2: Ternary diagram comparing grain size of sediments found on sea ice (filled circles) and those from shelf areas shallower than 30 meters (squares) (Reimnitz et al., in press)

Figure 3: Map of sample locations (dots indicate locations of sea ice samples, squares indicate locations of glacial samples)

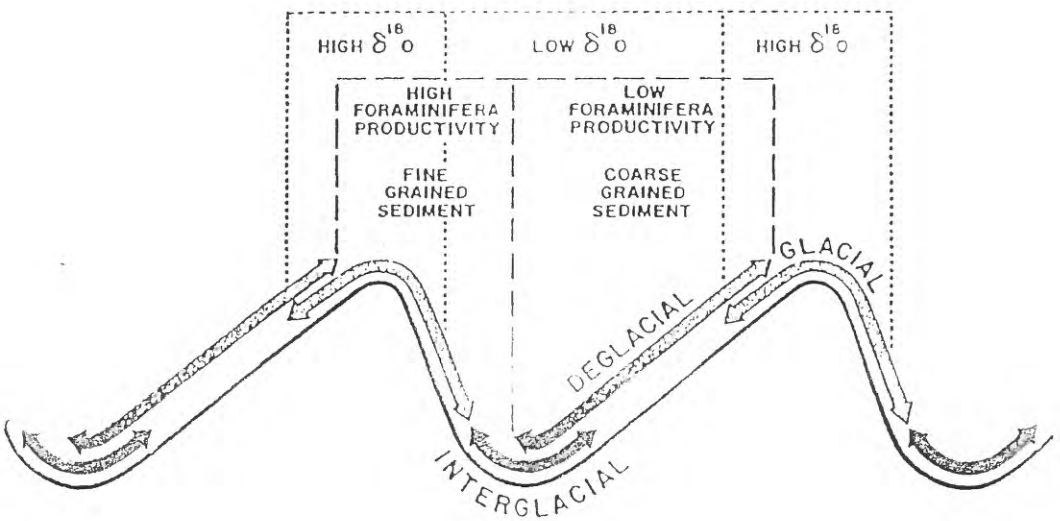

Figure 4: Schematic diagram correlating sedimentation with climate cycles (Clark and Morris, 1985)

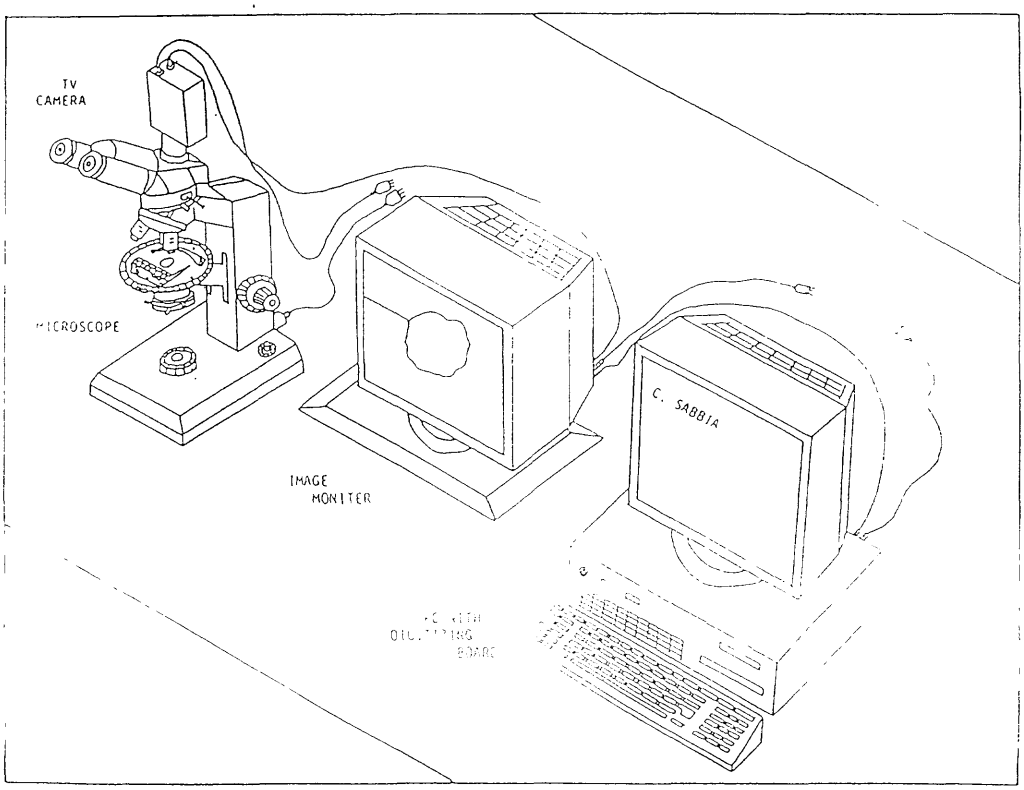

Figure 5: Diagram of automated image analysis system (Cai, 1994)

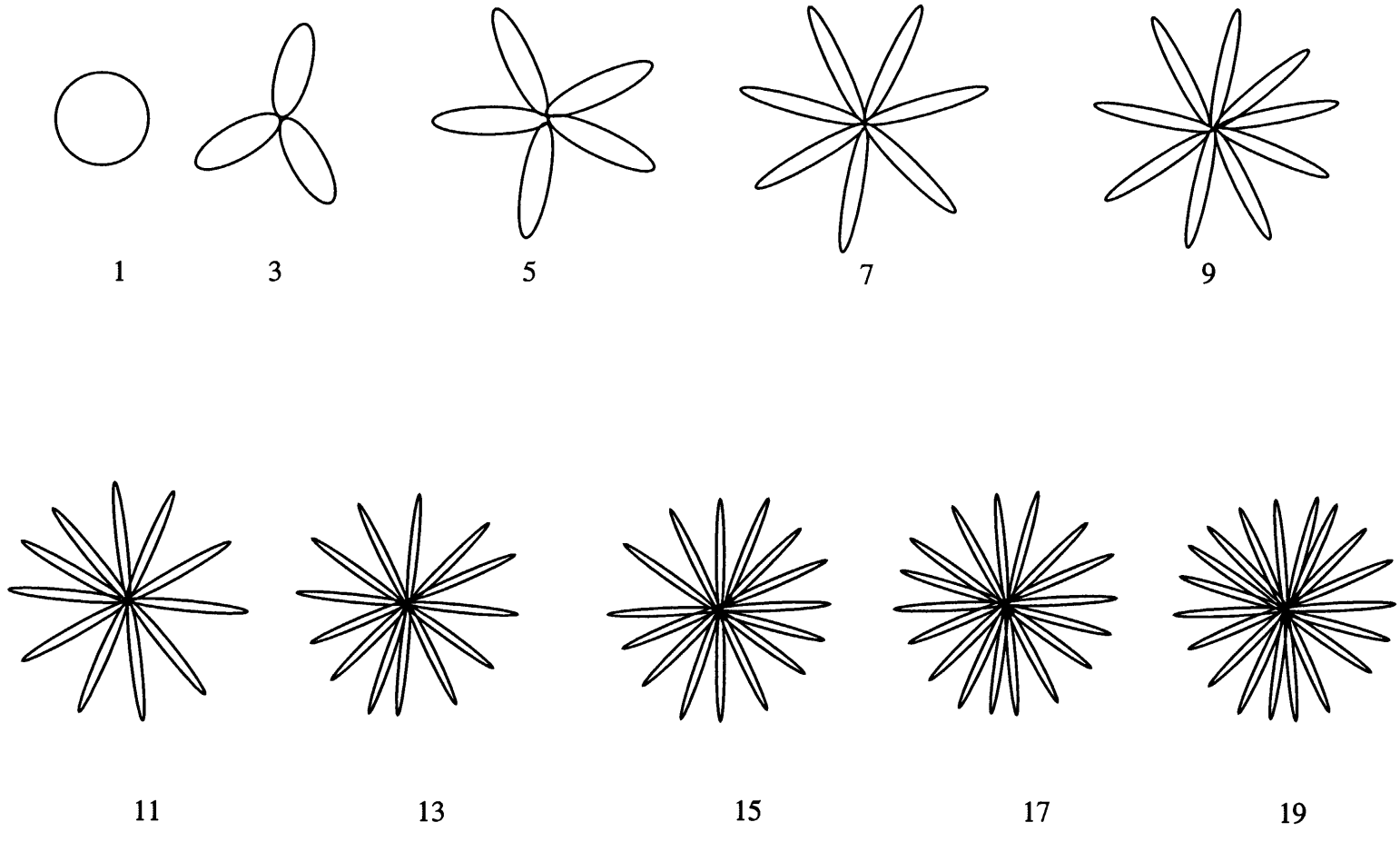

Figure 6: Graphic representation of harmonics

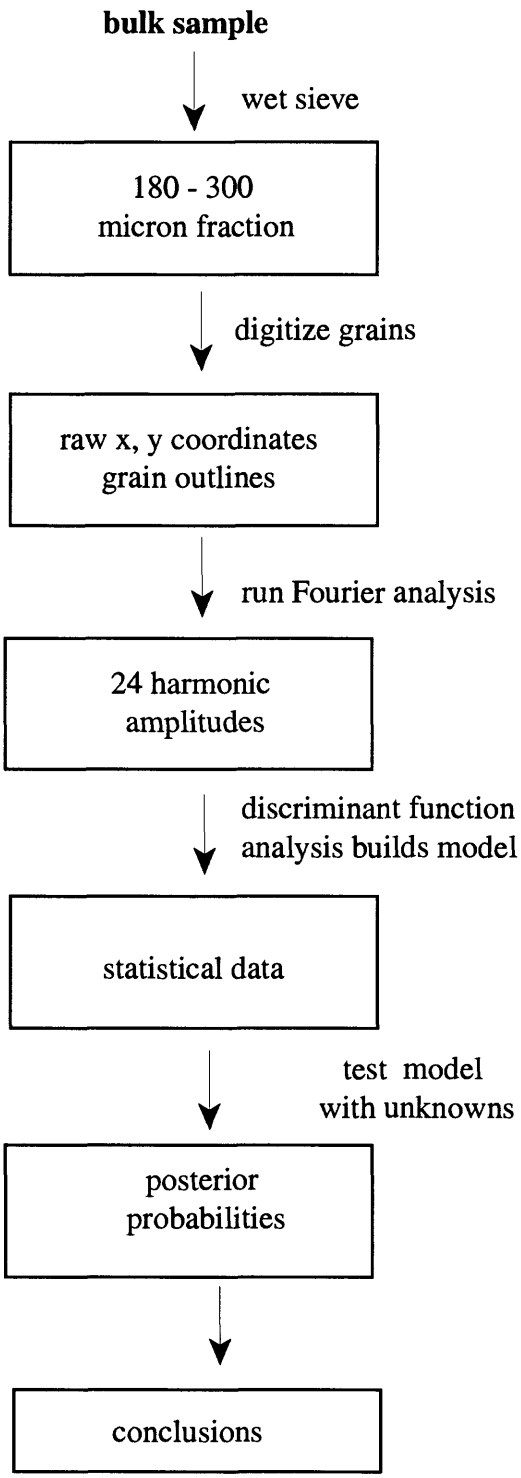

Figure 7: Analytical procedure for shape analysis

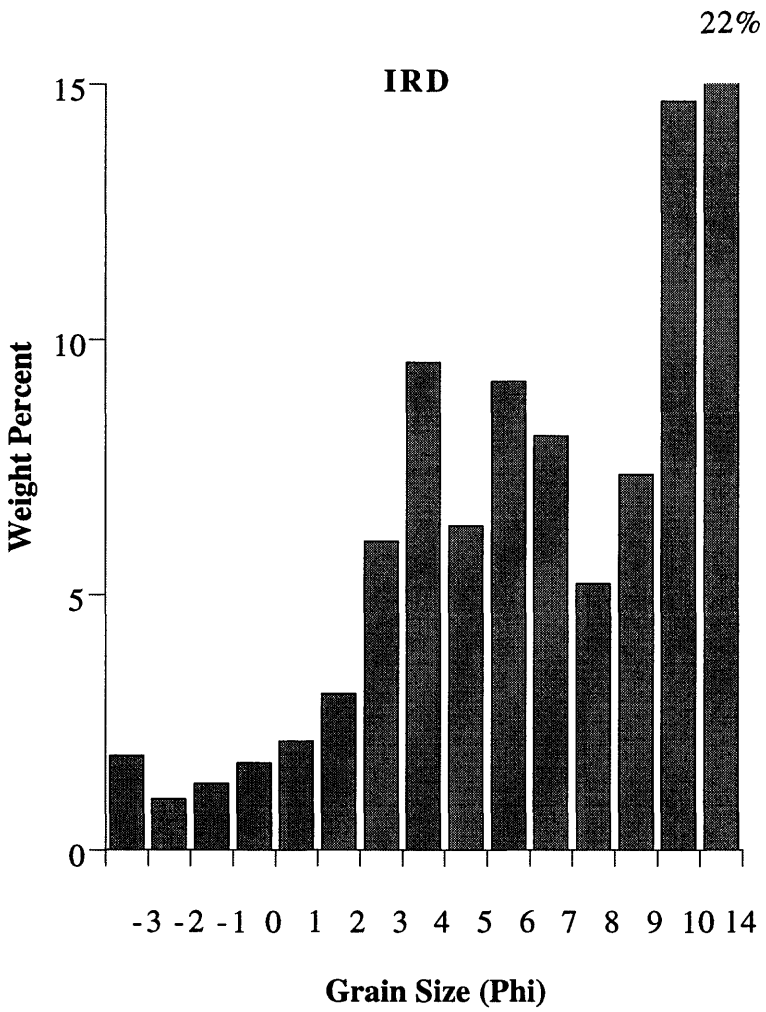

Figure 8: Single phi histogram of IRD

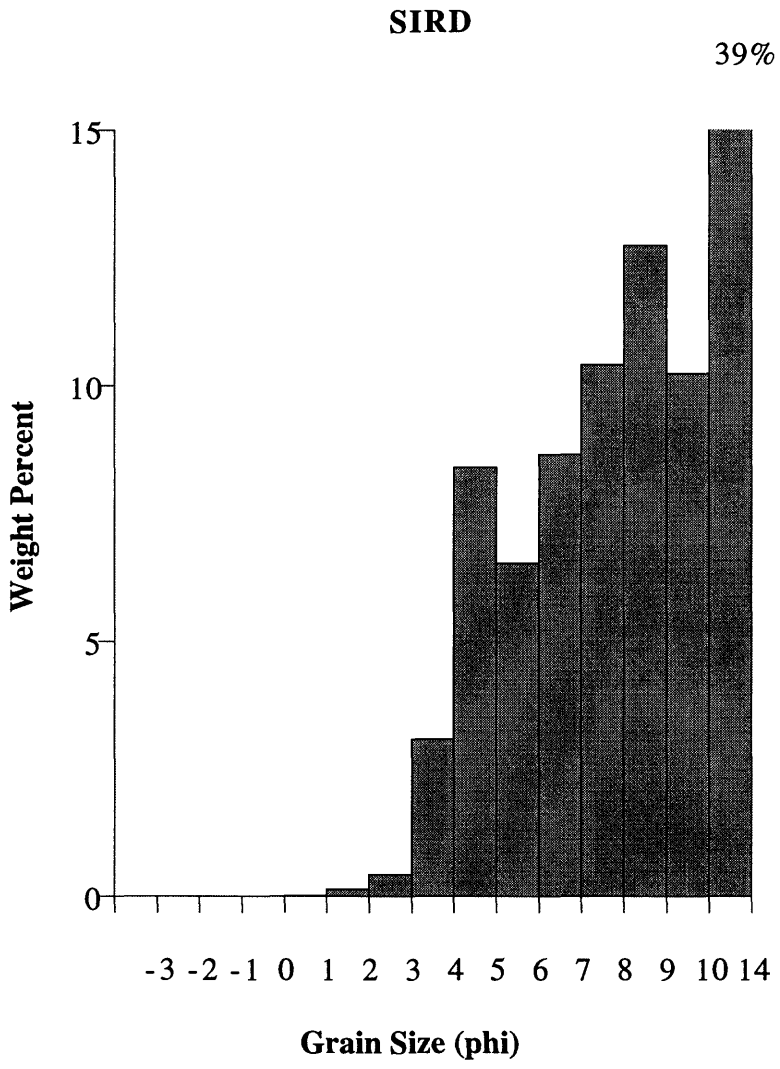

Figure 9: Single phi histogram of SIRD

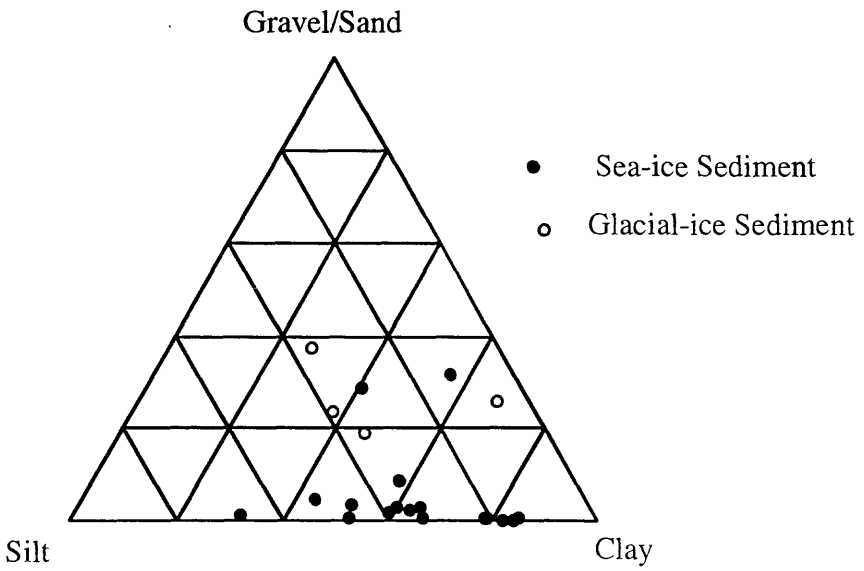

Figure 10: Ternary diagram comparing grain size of sea-ice sediment (filled circles) and glacial-ice sediment (open circles)

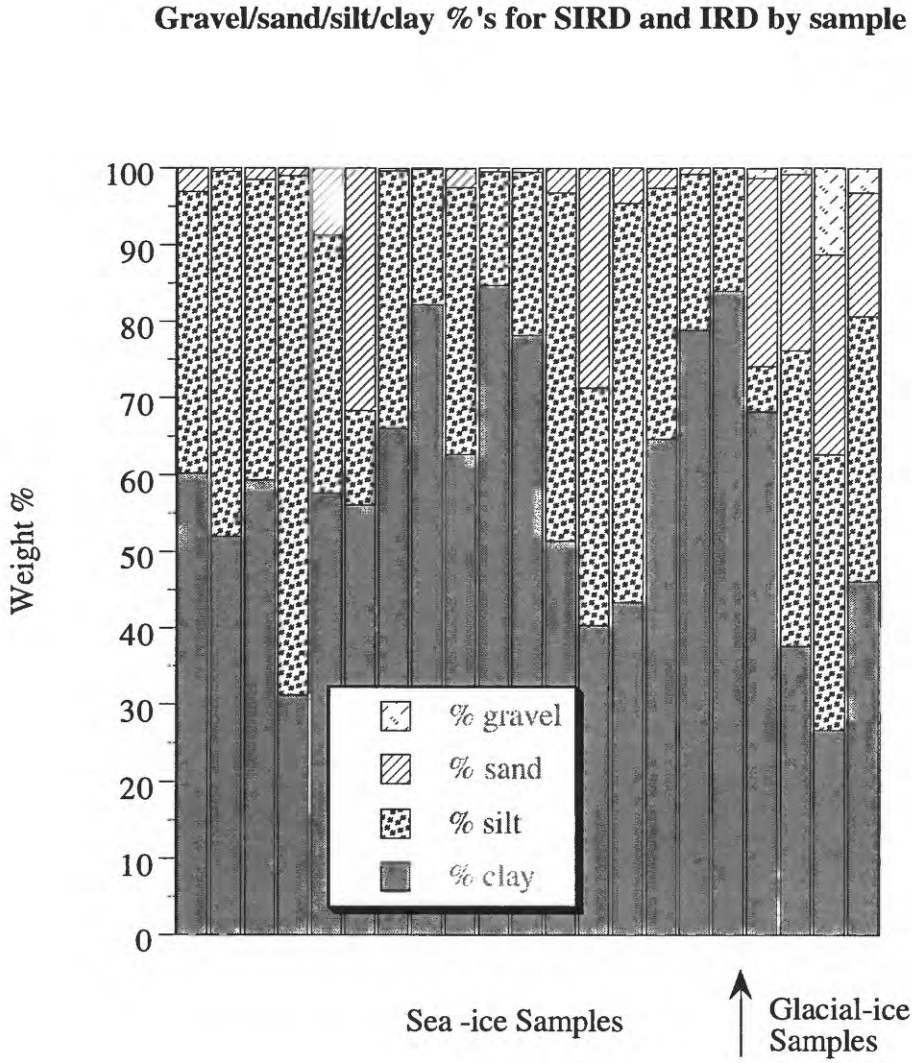

Figure 11: Bar graph comparing grain size data for SIRD and IRD

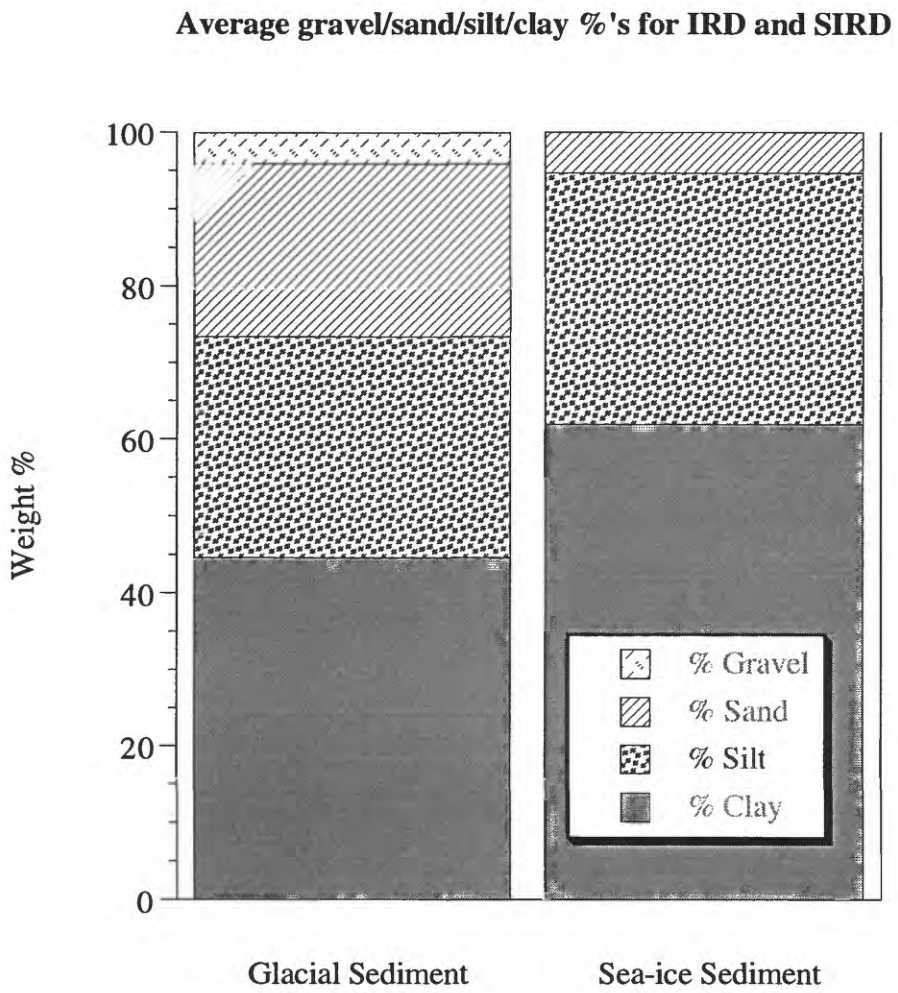

Figure 12: Bar graph comparing averaged grain size data for IRD and SIRD

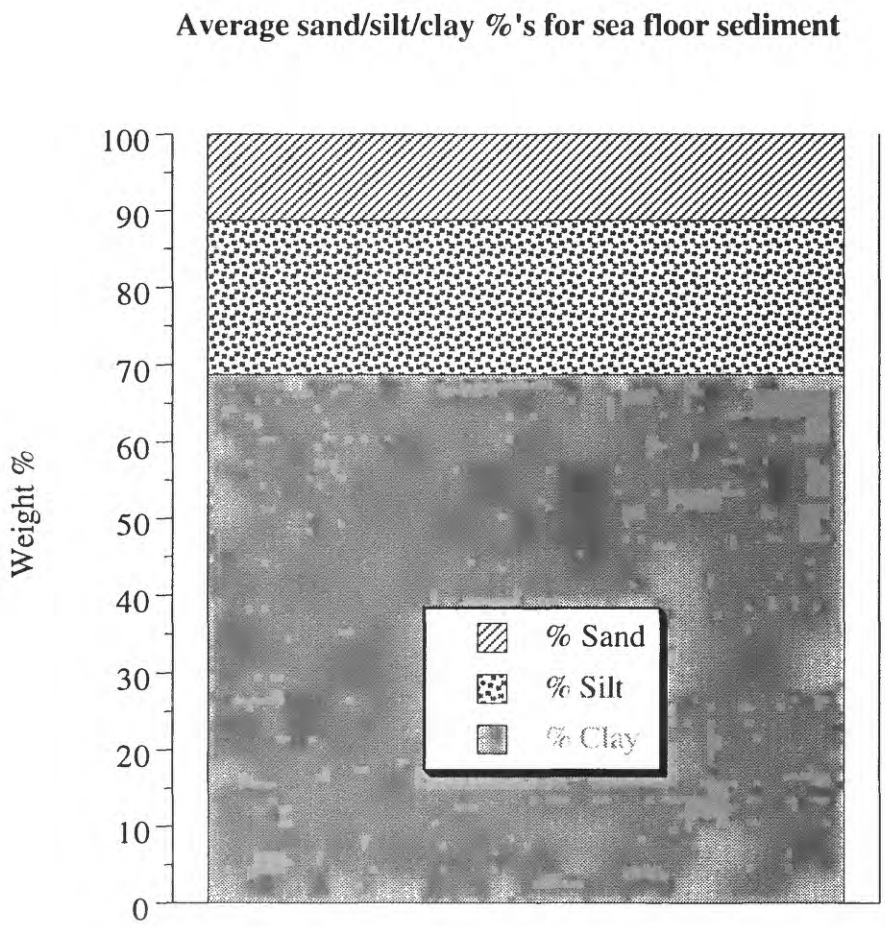

Figure 13: Bar graph showing grain size data for sea floor sediment

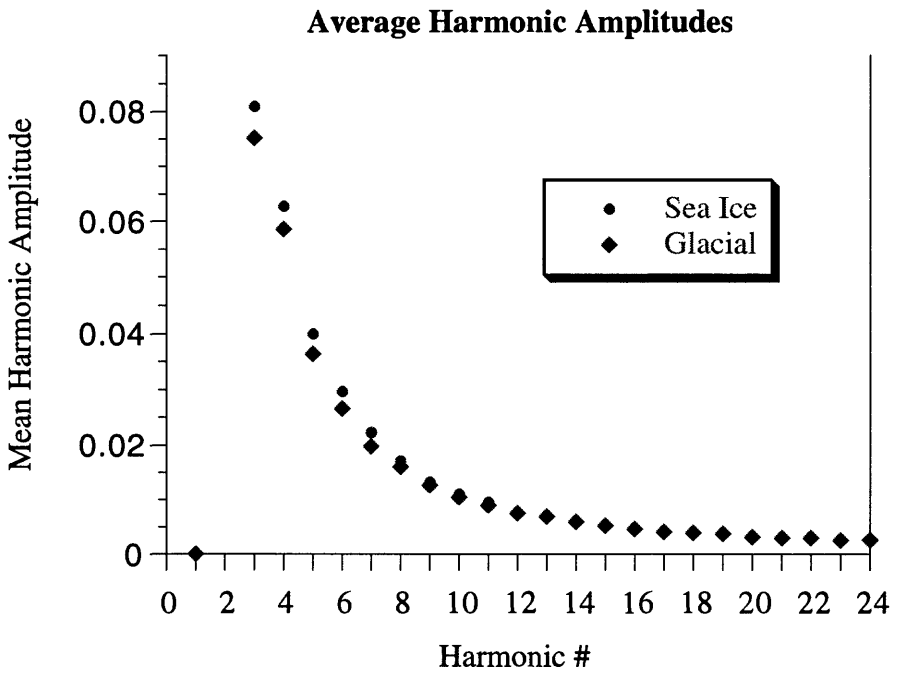

Figure 14: Graph of 2-24 harmonics

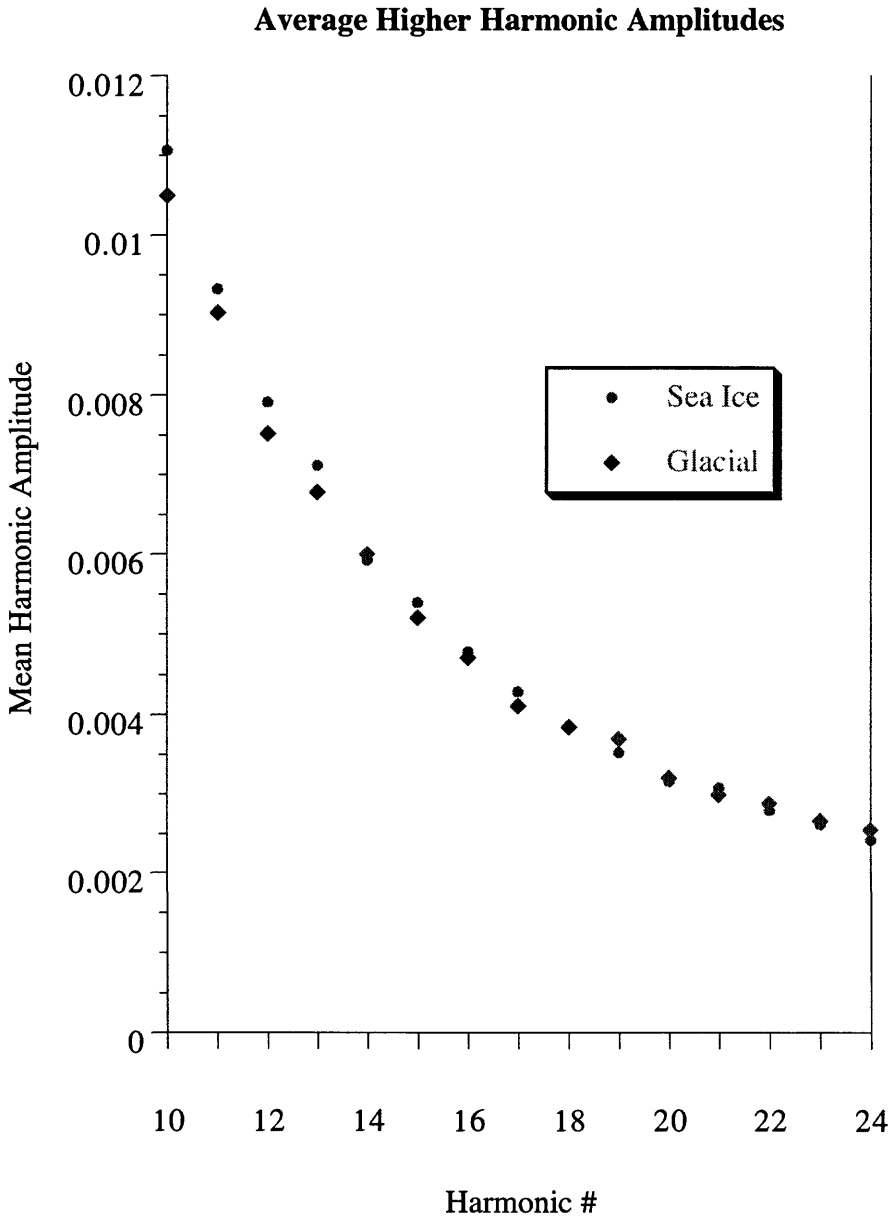

Figure 15: Graph of 10-24 harmonics

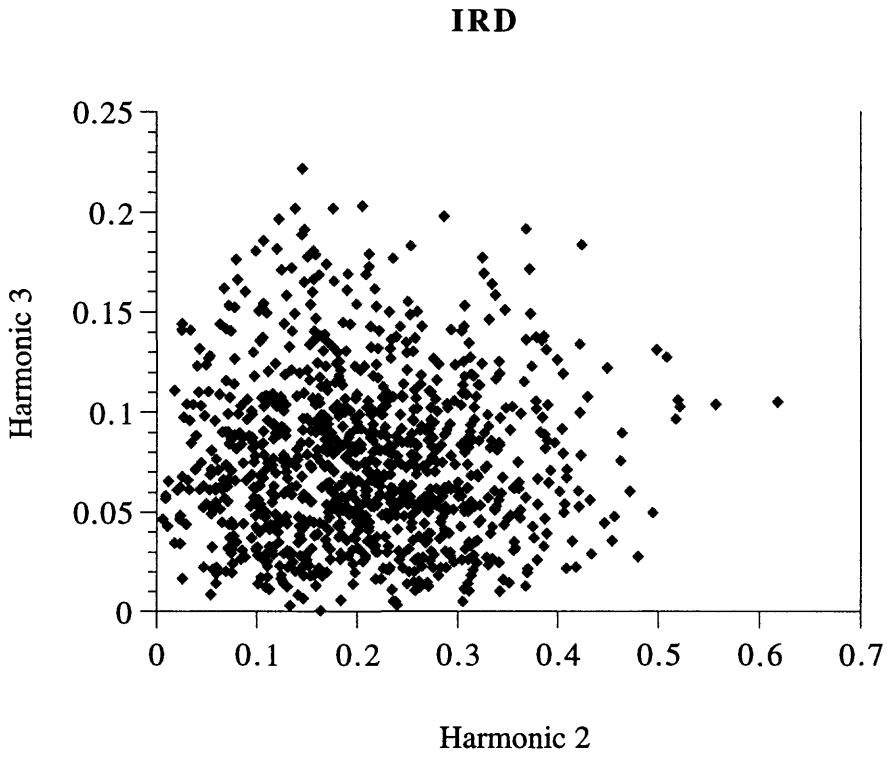

Figure 16a: Scatterplot of harmonic #2 vs. harmonic #3 for IRD

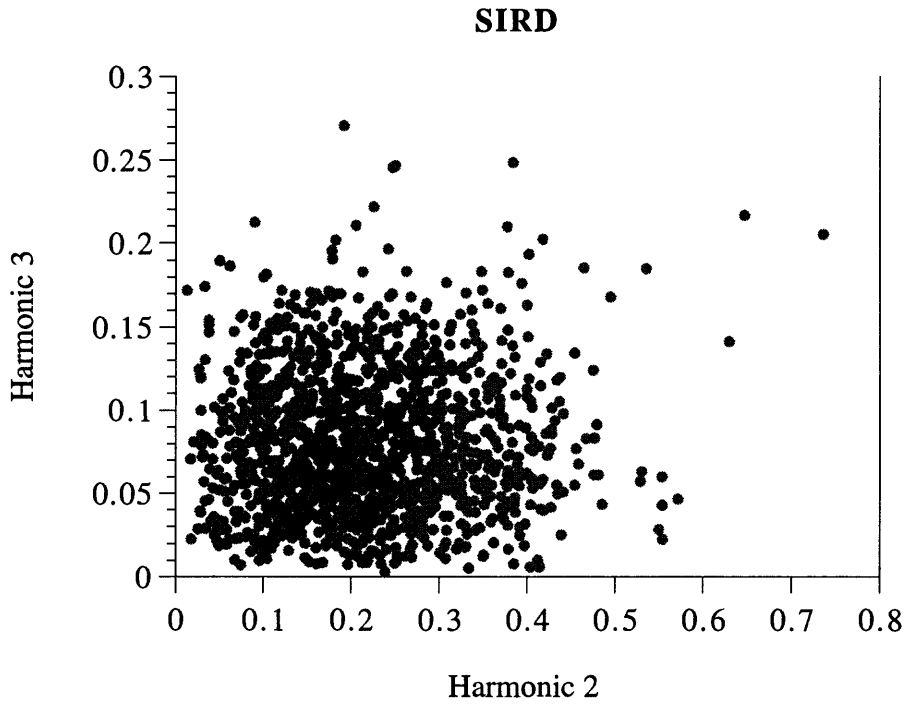

Figure 16b: Scatterplot of harmonic #2 vs. harmonic #3 for SIRD

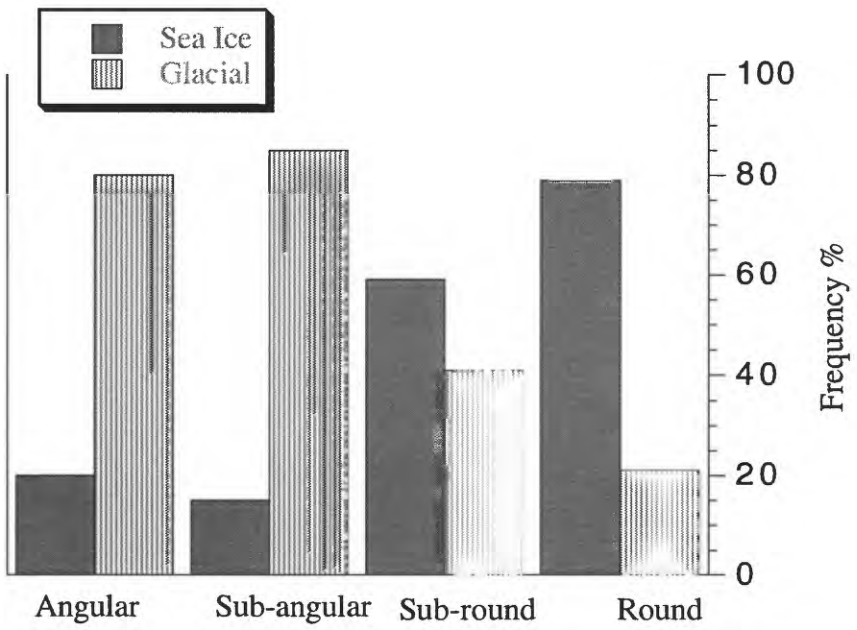

Figure 17: Frequency percentage graph of grain shapes

Prefix	Sample #	Latitude (N)	Longitude (W/E)	Sample Type
AOS 94-	207-1	70°00'	168°44' W	sea ice
AOS 94-	208-1	72°00'	168°50' W	sea ice
AOS 94-	212-1	75°48'	171°56.' W	sea ice
AOS 94-	212-2	75°57'	171°57.5' W	sea ice
AOS 94-	214-1	77°49'	176°21' W	sea ice
AOS 94-	215-1	78°07'	176°44' W	sea ice
AOS 94-	215-E3	78°07'	176°44' W	sea ice
AOS 94-	218-1	80°08'	173°22' W	sea ice
AOS 94-	220-1	80°20'	178°41' W	sea ice
AOS 94-	222-1	81°34'	176°58' E	sea ice
AOS 94-	223-1	82°27'	175°51' E	sea ice
AOS 94-	224-1	83°10'	174°05' E	sea ice
AOS 94-	226-1	84°50'	170°42' E	sea ice
AOS 94-	227-1	85°54'	166°50' E	sea ice
AOS 94-	232-1	89°00'	137°40' E	sea ice
AOS 94-	234-1	89°59.'	035°44.' E	sea ice
AOS 94-	235-1	89°41'	011°24' E	sea ice
BC	8	78°07.68'	176°44.67' W	sea floor
BC	12	79°59.32'	174°17.32' W	sea floor
BC	16	80°20.33'	178°42.71' W	sea floor
BC	26	88°48.60'	142°58.90' E	sea floor
BC	28	88°52.40'	140°10.80' E	sea floor
BC	30	88°59.97'	137°29.70' E	sea floor
	interval (cm)			
P26	75-85	74°00.00'	157°36.54'W	glacial
P26	280-285	74°48.84'	157°36.05'W	glacial
P26	295-300	74°48.84'	157°36.05'W	glacial
P27	605-615	74°48.84'	157°36.05'W	glacial

Table 2: Coordinates of sample sites

Sample	gravel %	sand %	silt %	clay %	median (phi)	mean sz (phi)	sort	skew.	kurt.
P27	1.30	24.62	5.92	68.16	11.31	9.48	4.53	-0.56	0.51
P26-300	0.82	23.00	38.63	37.56	6.35	6.31	2.88	-0.11	0.74
P26-280	11.17	26.10	36.08	26.65	5.21	5.08	4.19	-0.19	1.00
P26-75	3.19	16.15	34.58	46.08	7.63	7.64	4.08	-0.07	0.99
Average	4.12	22.47	28.80	44.61	7.63	7.13	3.92	-0.23	0.81

Note: statistics according to Folk and Ward (1957)

Table 3: IRD grain size data

Phi Interval	P27 605	P26 300	P26 280	P26 75	Average
-3	0.00	0.00	7.35	0.00	1.84
-2	0.00	0.00	1.55	2.41	0.99
-1	1.30	0.82	2.26	0.78	1.29
0	1.18	1.68	2.33	1.59	1.70
1	1.48	2.11	3.29	1.62	2.13
2	2.27	3.69	4.44	1.89	3.07
3	7.17	5.88	6.42	4.67	6.04
4	12.54	9.63	9.63	6.39	9.55
5	5.56	4.70	10.36	4.72	6.34
6	0.00	16.32	10.49	9.89	9.18
7	0.19	14.87	8.05	9.27	8.10
8	0.19	2.75	7.18	10.70	5.21
9	2.77	11.19	6.36	9.05	7.34
10	6.10	25.49	19.55	7.48	14.66
14	59.34	0.88	0.74	29.55	22.63
Weight percent of the entire sample determined by sieving and pipetting					

Table 4: 1 phi IRD grain size data by sample

Sample	gravel %	sand %	silt %	clay %	median (phi)	mean sz (phi)	sort	skew.	kurt.
207-1	0	3.06	36.72	60.23	8.45	8.37	2.66	0.00	1.34
208-1	0	0.48	47.52	52.00	8.07	8.19	2.30	0.16	1.33
212-1	0	1.48	39.18	59.34	8.54	8.65	2.43	0.08	1.15
212-2	0	0.96	67.87	31.17	4.97	6.60	2.89	0.79	0.81
214-1	0	8.64	33.65	57.71	8.39	8.49	3.32	0.03	0.72
215-E3	0	31.67	12.20	56.13		8.14	3.79	-0.15	
215-1	0	0.42	33.54	66.05	9.44	9.44	2.85	-0.01	0.75
218-1	0	0.17	17.59	82.24	10.46	10.40	2.36	-0.08	0.82
220-1	0	2.56	34.73	62.70	9.06	9.08	2.90	0.00	0.76
222-1	0	0.45	14.77	84.78	13.81	11.67	2.48	-1.15	0.99
223-1	0	0.58	21.24	78.18	9.83	9.70	2.53	-0.09	1.18
224-1	0	3.24	45.34	51.42	8.11	9.06	3.49	0.26	0.57
226-1	0	28.70	30.93	40.37	6.60	7.15	3.42	0.28	0.64
227-1	0	4.61	51.92	43.47	7.51	7.99	2.95	0.24	0.88
232-1	0	2.63	32.70	64.66	9.54	9.45	3.20	-0.06	0.66
234-1	0	0.83	20.28	78.90	11.21	10.71	2.70	-0.30	0.75
235-1	0	0.00	15.94	84.06	10.21	10.30	2.22	0.02	0.84
Average	0.00	5.32	32.71	61.97	9.01	9.02	2.85	0.00	0.89
Averages omitting 215-E3 & 226-1									
		2.01	34.20	63.79	9.17	9.21	2.75	-0.01	0.90
Note: statistics according to Folk and Ward (1957)									

Table 5: SIRD grain size data

Phi Interval	207-1	208-1	212-1	212-2	214-1	215-1	218-1	220-1	222-1	223-1	224-1	226-1	227-1	232-1	234-1	235-1	Average
-3.00	0.00	0.00	0.00	0.00	0.00	0.00	0.00	0.00	0.00	0.00	0.00	0.00	0.00	0.00	0.00	0.00	0.00
-2.00	0.00	0.00	0.00	0.00	0.00	0.00	0.00	0.00	0.00	0.00	0.00	0.00	0.00	0.00	0.00	0.00	0.00
-1.00	0.00	0.00	0.00	0.00	0.00	0.00	0.00	0.00	0.00	0.00	0.00	0.00	0.00	0.00	0.00	0.00	0.00
0.00	0.00	0.00	0.00	0.00	0.00	0.00	0.00	0.00	0.00	0.00	0.00	0.00	0.00	0.00	0.00	0.00	0.00
1.00	0.00	0.00	0.00	0.00	0.00	0.00	0.00	0.00	0.08	0.00	0.00	0.04	0.03	0.00	0.14	0.00	0.02
2.00	1.04	0.08	0.28	0.01	0.00	0.01	0.01	0.11	0.03	0.01	0.15	0.16	0.26	0.04	0.05	0.00	0.14
3.00	1.33	0.11	0.42	0.09	0.00	0.05	0.02	0.44	0.08	0.03	0.62	2.42	0.98	0.08	0.20	0.00	0.43
4.00	0.68	0.29	0.78	0.86	8.64	0.36	0.13	2.01	0.28	0.55	2.47	26.08	3.34	2.52	0.44	0.00	3.09
5.00	8.15	3.62	4.11	50.74	8.41	3.93	2.25	7.07	2.27	2.95	9.38	11.60	10.41	6.91	1.42	1.24	8.40
6.00	7.39	12.06	7.67	9.82	0.00	8.56	0.56	6.46	3.41	4.52	10.60	6.28	13.60	8.09	3.74	1.59	6.52
7.00	0.88	20.74	9.86	3.78	5.61	10.87	5.24	15.68	2.84	7.87	12.76	5.80	14.17	12.64	5.51	4.25	8.66
8.00	20.30	11.10	17.54	3.53	19.63	10.18	9.54	5.53	6.25	5.90	12.60	7.25	13.74	5.06	9.61	8.86	10.41
9.00	21.43	29.19	17.26	6.93	19.63	11.33	12.54	11.99	8.52	5.11	8.30	7.41	11.72	10.45	6.40	15.41	12.73
10.00	14.66	4.58	16.99	5.41	2.80	10.64	13.47	11.99	4.26	27.92	3.84	7.73	6.80	7.76	9.43	15.59	10.24
14.00	24.13	18.23	25.09	18.84	35.28	44.08	56.24	38.73	72.00	45.15	39.28	25.23	24.96	46.46	63.07	53.06	39.36

Weight percent of the entire sample determined by sieving and pipetting

Table 6: 1 phi SIRD grain size data by sample

Sample	gravel	sand	silt	clay	median	mean sz	sort	skewness	kurtosis
	%	%	%	%	(phi)	(phi)			
BC-8	0	10.89	23.65	65.45	9.06	8.40	2.91	-0.37	1.00
BC-12	0	14.26	23.77	61.98	8.91	8.11	3.25	-0.41	0.88
BC-16	0	19.19	21.43	59.38	8.96	7.99	3.63	-0.44	0.78
BC-26	0	16.46	25.98	57.57	8.74	7.96	3.24	-0.34	0.76
BC-28	0	5.54	13.49	80.97	9.86	9.72	2.11	-0.31	1.29
BC-30	0	0.96	11.83	87.21	10.05	9.95	1.78	-0.27	1.19
Average	0.00	11.21	20.03	68.76	9.26	8.69	2.82	-0.36	0.98
Note: statistics according to Folk and Ward (1957)									

Table 7: Sea floor sediment grain size data

	Predicted Group Membership		
Actual Group	**# of grains**	**Sea Ice**	**Glacial**
Sea Ice	1220	**685**	535
Glacial	1144	496	**648**
Sea Ice	1220	56%	44%
Glacial	1144	43%	57%

Classified Correctly	
Sea Ice	56%
Glacial	57%

Table 8: Classification of sediment type based on grain shape data

Harmonic #		Glacial	Range	Sea Ice	Range	Harmonic #		Glacial	Range	Sea Ice	Range
	Min	0.005679	0.612969	0.013795	0.723159		Min	0.000069	0.02671	0.000081	0.033632
2	Max	0.618648		0.736954		14	Max	0.026779		0.033713	
	Ave	0.210893484		0.217660579	0.006767095		Ave	0.005990724		0.005922764	-6.7959E-05
	Min	0.000696	0.221102	0.002868	0.267709		Min	0.000213	0.02308	0.000102	0.033414
3	Max	0.221798		0.270577		15	Max	0.023293		0.033516	
	Ave	0.075255173		0.080830825	0.005575652		Ave	0.005206951		0.005395761	0.00018881
	Min	0.000808	0.201026	0.001512	0.295805		Min	0.000066	0.020794	0.000122	0.036072
4	Max	0.201834		0.297317		16	Max	0.02086		0.036194	
	Ave	0.058552003		0.062827847	0.004275844		Ave	0.004712248		0.004789073	7.68253E-05
	Min	0.001685	0.152482	0.00131	0.211563		Min	0.000054	0.019039	0.000155	0.030129
5	Max	0.154167		0.212873		17	Max	0.019093		0.030284	
	Ave	0.036355077		0.039898508	0.003543431		Ave	0.004107877		0.004291816	0.000183938
	Min	0.00047	0.101022	0.001062	0.135074		Min	0.000049	0.013355	0.000074	0.027106
6	Max	0.101492		0.136136		18	Max	0.013404		0.02718	
	Ave	0.026475183		0.029576641	0.003101457		Ave	0.003840487		0.003840629	1.42289E-07
	Min	0.000447	0.078118	0.000487	0.131749		Min	0.000065	0.01582	0.000062	0.020207
7	Max	0.078565		0.132236		19	Max	0.015885		0.020269	
	Ave	0.019736944		0.022243345	0.002506401		Ave	0.003695118		0.003523391	-0.00017173
	Min	0.000307	0.056598	0.000432	0.089095		Min	0.000036	0.014305	0.000058	0.019469
8	Max	0.056905		0.089527		20	Max	0.014341		0.019527	
	Ave	0.016037455		0.017078523	0.001041067		Ave	0.003214201		0.003166627	-4.7573E-05
	Min	0.000132	0.055334	0.000311	0.06979		Min	0.000026	0.014434	0.000097	0.01488
9	Max	0.055466		0.070101		21	Max	0.01446		0.014977	
	Ave	0.012696585		0.013265269	0.000568684		Ave	0.002993696		0.003080122	8.64265E-05
	Min	0.000278	0.044277	0.00018	0.086012		Min	0.000066	0.014551	0.000063	0.014347
10	Max	0.044555		0.086192		22	Max	0.014617		0.01441	
	Ave	0.010501984		0.01106776	0.000565776		Ave	0.00288223		0.002797859	-8.4372E-05
	Min	0.000103	0.032184	0.000119	0.054744		Min	0.000138	0.012779	0.000029	0.012698
11	Max	0.032287		0.054863		23	Max	0.012917		0.012727	
	Ave	0.009025617		0.00932454	0.000298923		Ave	0.0026625		0.002622212	-4.0288E-05
	Min	0.000189	0.02768	0.000191	0.052188		Min	0.000069	0.010825	0.000028	0.012705
12	Max	0.027869		0.052379		24	Max	0.010894		0.012733	
	Ave	0.007514893		0.007916728	0.000401834		Ave	0.002543944		0.002423558	-0.00012039
	Min	0.000119	0.025535	0.000229	0.048239						
13	Max	0.025654		0.048468							
	Ave	0.00677988		0.007120404	0.000340524						

Table 9: Harmonic amplitude data for SIRD and IRD

Surface Feature	Energy Level	Process	Environments
Mechanical Breakage Features			
high relief	high	mechanical stress	glacial
low relief	low	abrasion/chemical	subaqueous
small breakage blocks (<1 micron)	high	mechanical stress	glacial
large breakage blocks (>1 micron)	high	mechanical stress	glacial
small conchoidal fracture (<1 micron)	high	mechanical stress	glacial
large conchoidal fracture (>1 micron)	high	mechanical stress	glacial
step like fractures	high	mechanical stress	glacial
arc step-like fractures	high	mechanical stress	glacial
broken cleavage plates	high	mechanical stress	glacial
fractured surface	high	mechanical stress	glacial
Impact Features			
upturned plates	high	abrasion	wind transport
straight scratches (grooves)	med/high	abrasion	subaqueous/glacial
curved scratch (grooves)	med/high	abrasion	subaqueous/glacial
mechanical V's - impact pits	high	abrasion	subaqueous
abraded surface	high	abrasion	subaqueous
dish shaped concavities	high	abrasion	subaqueous/wind
angularity	high	mechanical stress	glacial
roundness	med/low	abrasion/ chemical alteration	subaqueous
Chemical Features			
oriented v-shaped etching	low	chemical alteration	subaqueous
etching pits	low	chemical alteration	subaqueous
silica precipitation	low	chemical alteration	subaqueous
irregular pitted (silica dissolution)	low	chemical alteration	subaqueous

Table 10: Environmental interpretation of surface features

Surface Feature	207-1	215-1	SIRD averages	280	300	IRD averages
shape (round, sub-r, sub-a, angular)	3.44	3.27	**3.4**	2.2	2.8	**2.5**
high/med/low relief	2.81	2.73	**2.8**	1.5	1.8	**1.7**
Mechanical Breakage Features						
small breakage blocks (<1 micron)	0.38	0.20	**0.3**	0.3	0.2	**0.2**
large breakage blocks (>1 micron)	0.38	0.40	**0.4**	1.5	0.6	**1.1**
small conchoidal fracture (<1 micron)	0.56	0.60	**0.6**	0.6	1.8	**1.2**
large conchoidal fracture (>1 micron)	0.63	0.67	**0.6**	1.3	1.8	**1.6**
fractured grain	0.38	0.47	**0.4**	1.5	1.7	**1.6**
step like fractures ((sub) parallel)	0.25	0.27	**0.3**	1.7	1.2	**1.4**
arc step-like fractures	0.31	0.27	**0.3**	1.3	1.2	**1.2**
broken cleavage plates	0.31	0.20	**0.3**	1.8	0.5	**1.1**
Impact Features						
upturned plates	1.75	2.27	**2.0**	1.5	1.5	**1.5**
mechanical V's - impact pits	1.00	1.46	**1.2**	1.5	0.5	**1.0**
dish shaped concavities	0.75	0.53	**0.6**	0.1	0.0	**0.0**
abraded surface	0.25	0.15	**0.2**	0.6	0.0	**0.3**
straight scratches (grooves)	0.25	0.00	**0.1**	0.0	0.0	**0.0**
curved scratch (grooves)	0.44	0.43	**0.4**	0.5	0.2	**0.3**
Chemical Features						
oriented v-shaped etching	0.00	1.93	**1.0**	0.1	1.2	**0.6**
etching pits	1.00	2.53	**1.8**	1.1	1.8	**1.5**
silica precipitation	2.38	2.60	**2.5**	1.7	1.8	**1.8**
irregular pitted (silica dissolution)	2.38	2.00	**2.2**	1.5	1.8	**1.7**

Notation:	**Shape**	**Relief**	**Surface features**	
	angular =1	high=1	none=0	0-2% coverage
	sub-angular=2	medium=2	present=1	2-25% coverage
	sub-round=3	low=3	common=2	25-75% coverage
	round=4		abundant=3	>75% coverage

Table 11: Averaged surface feature data

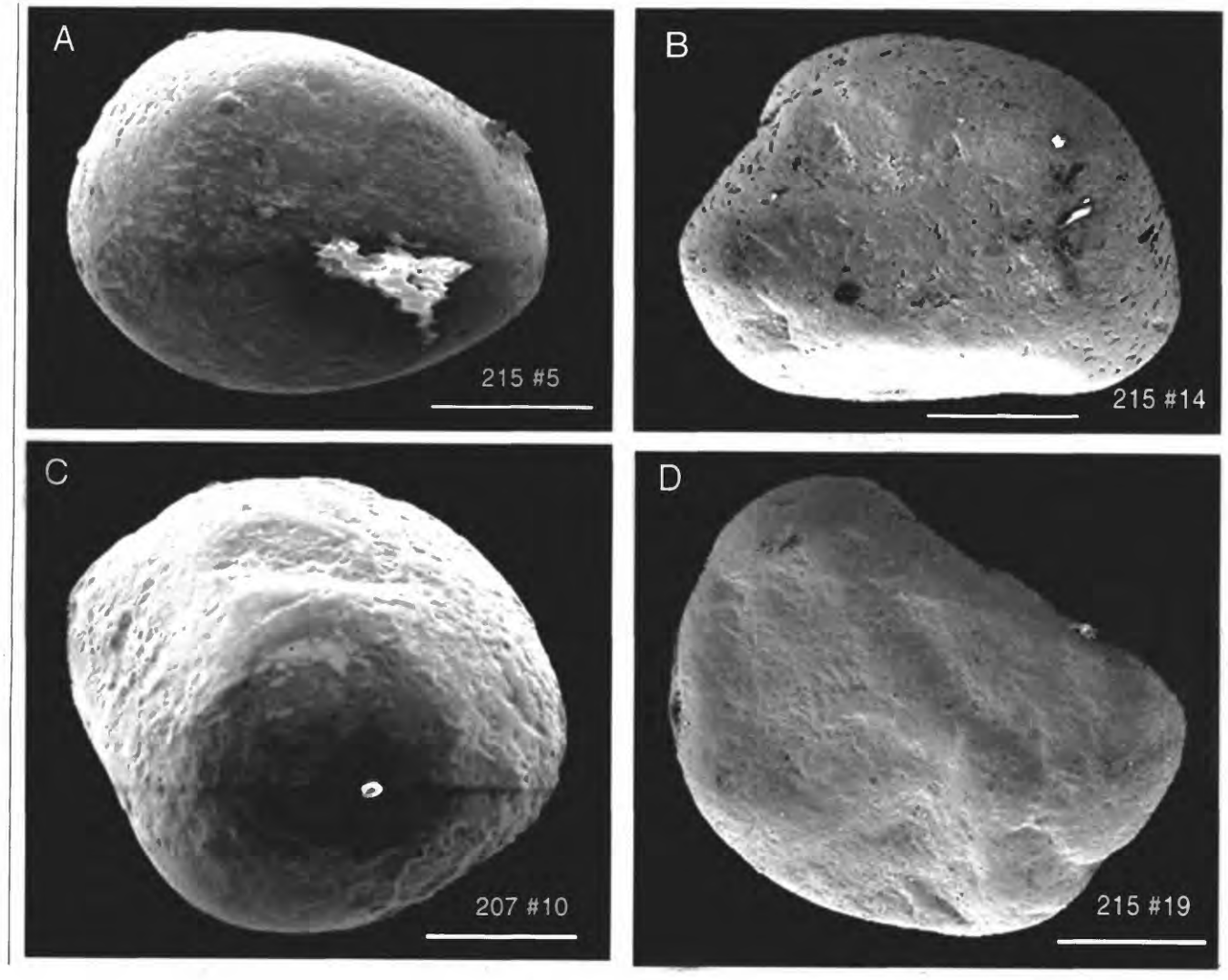

Plate 1: SEM images of sea ice grains

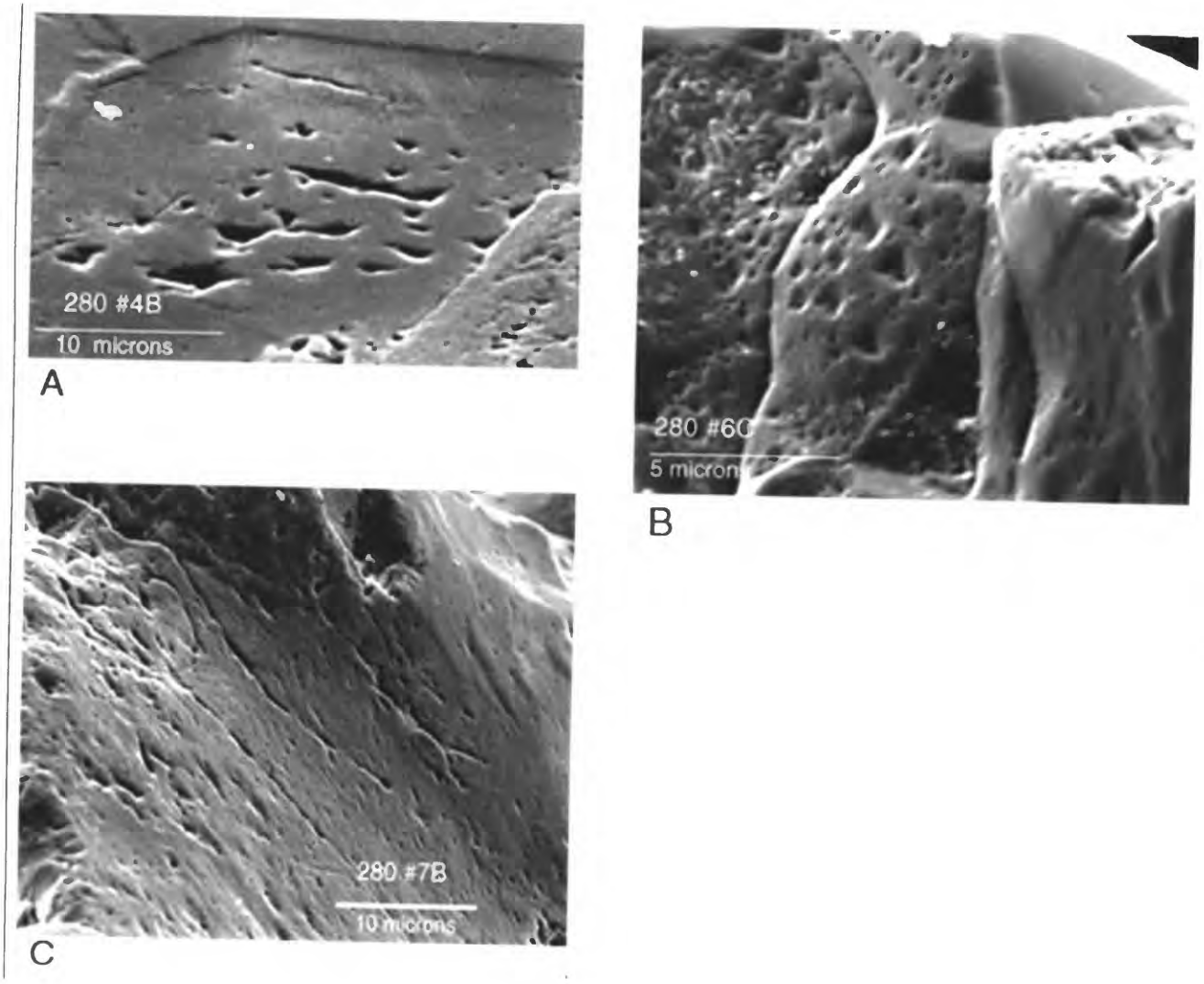

Plate 2: SEM images of impact pits

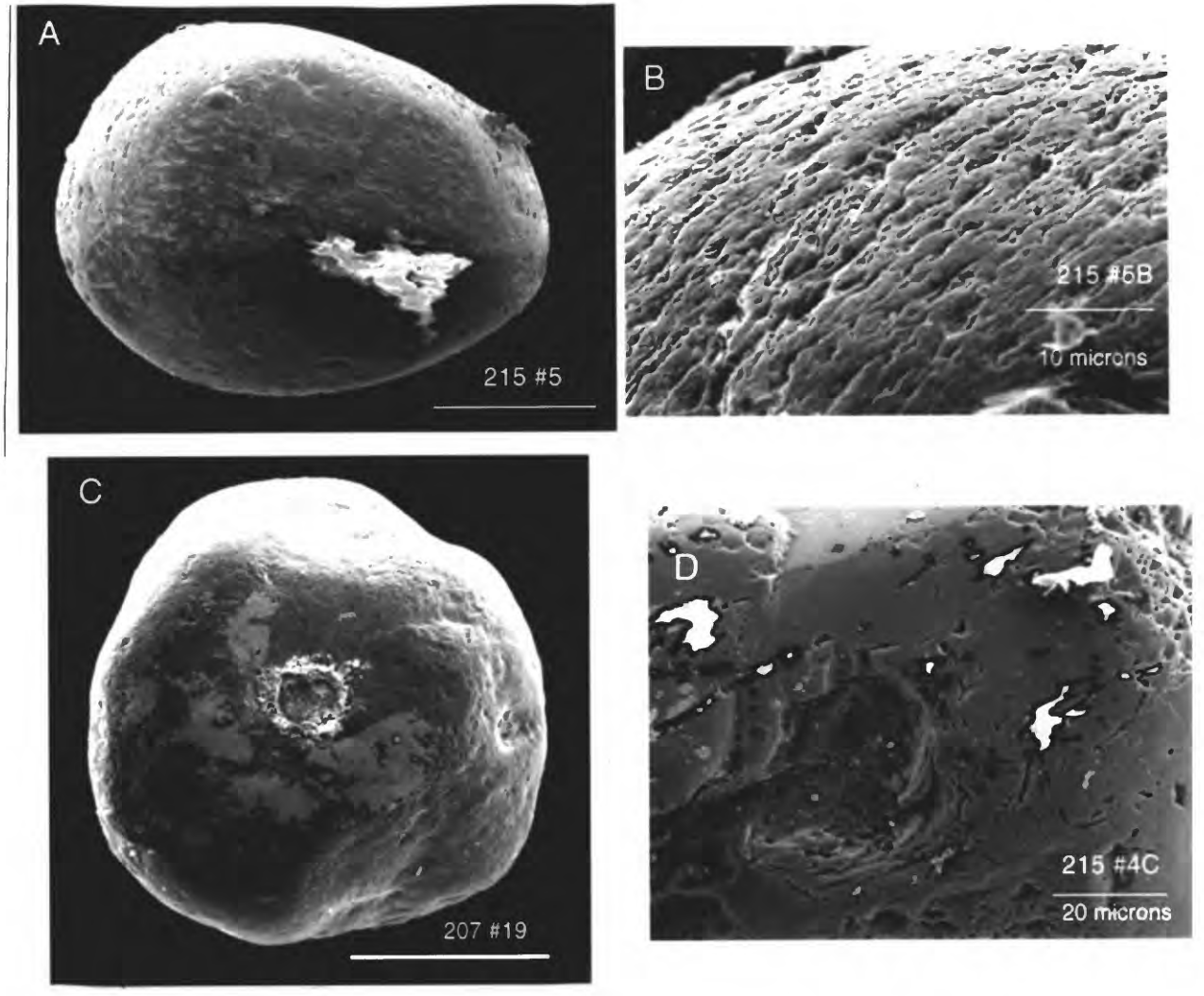

Plate 3: SEM image of: a. grain with upturned plates filled with silica precipitation, b. close up of upturned plate, c and d. dissolution pits

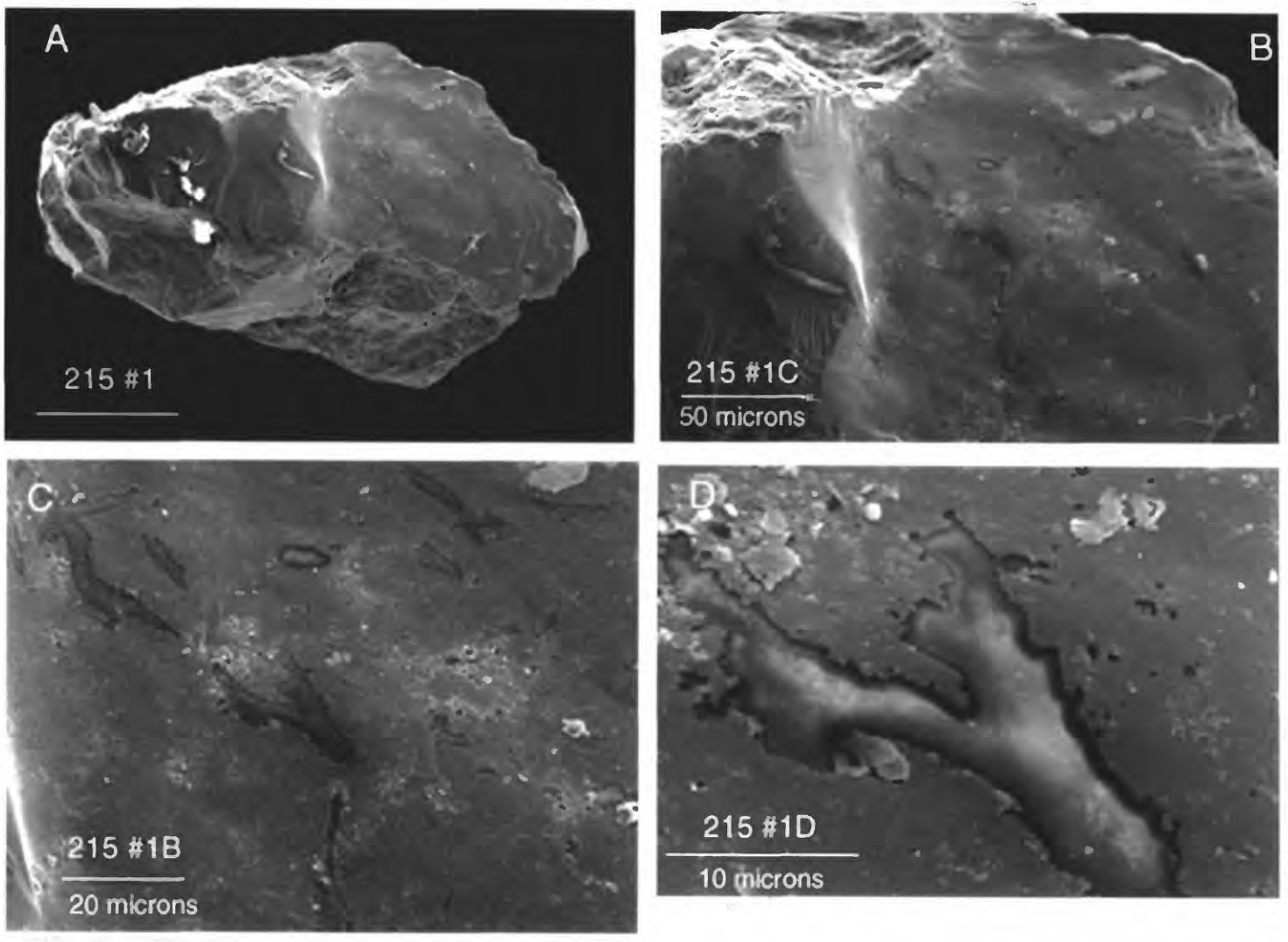

Plate 4: SEM images of irregular pitted surface due to silica dissolution

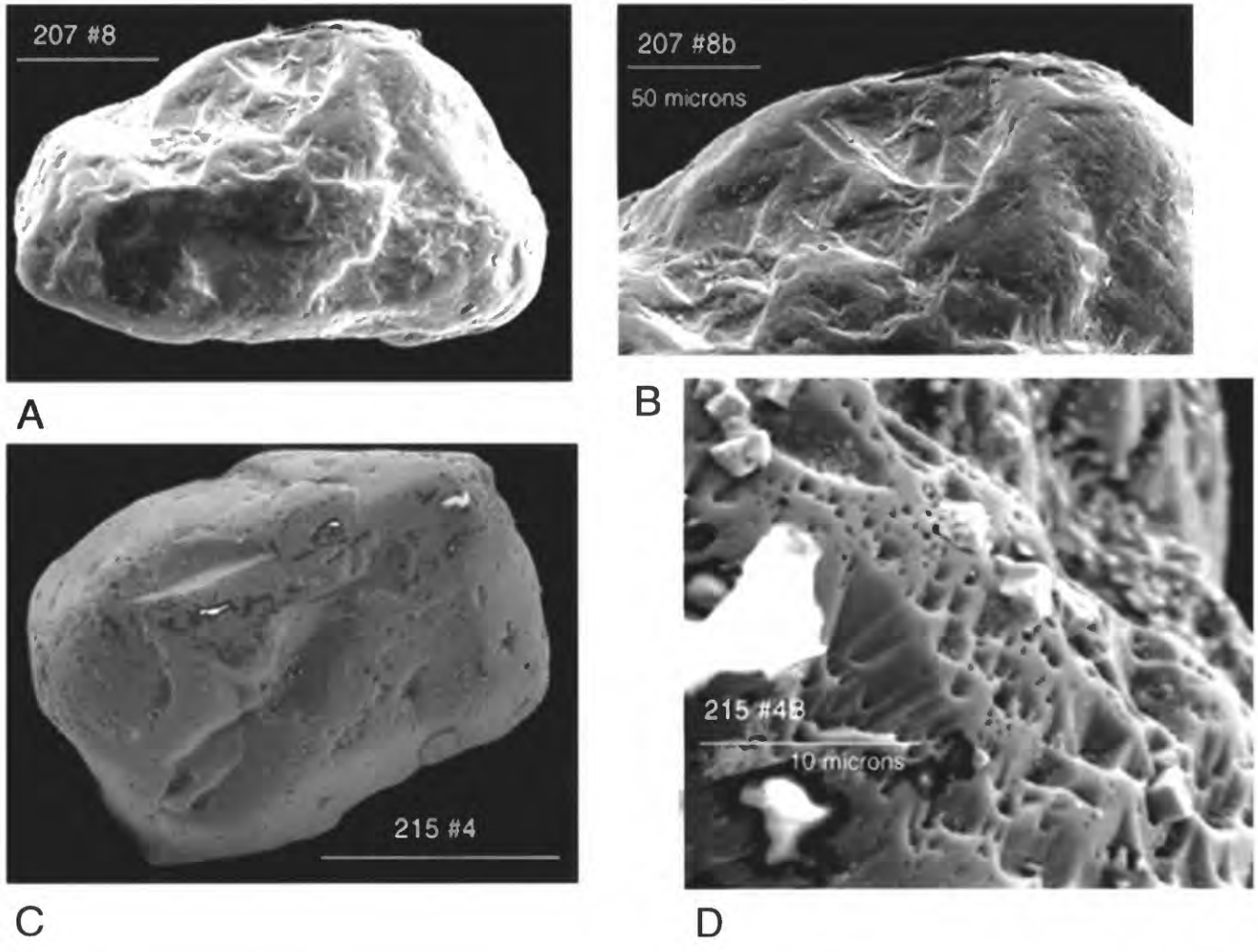

Plate 5: SEM images of oriented v-shaped etching

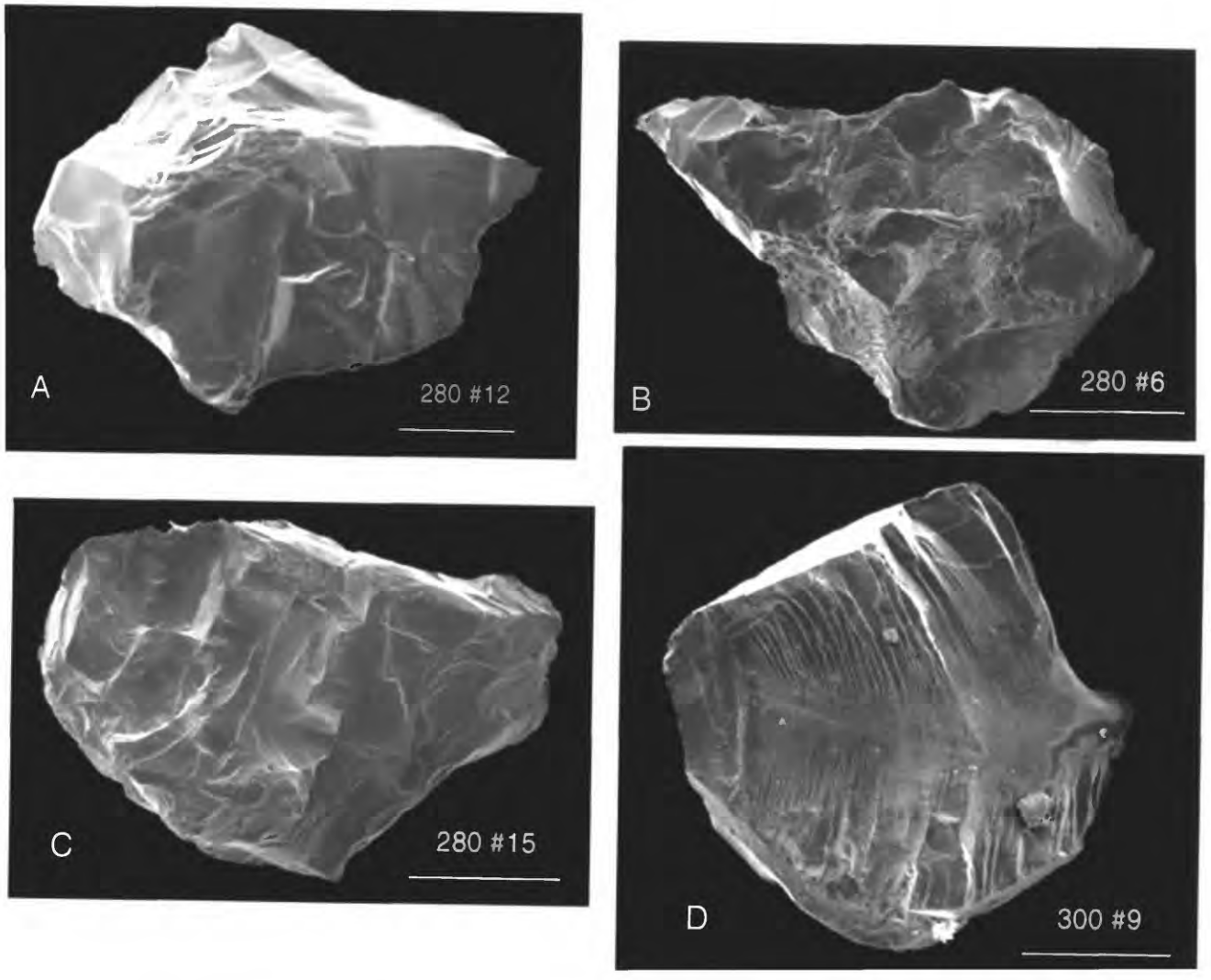

Plate 6: SEM images of glacial grains

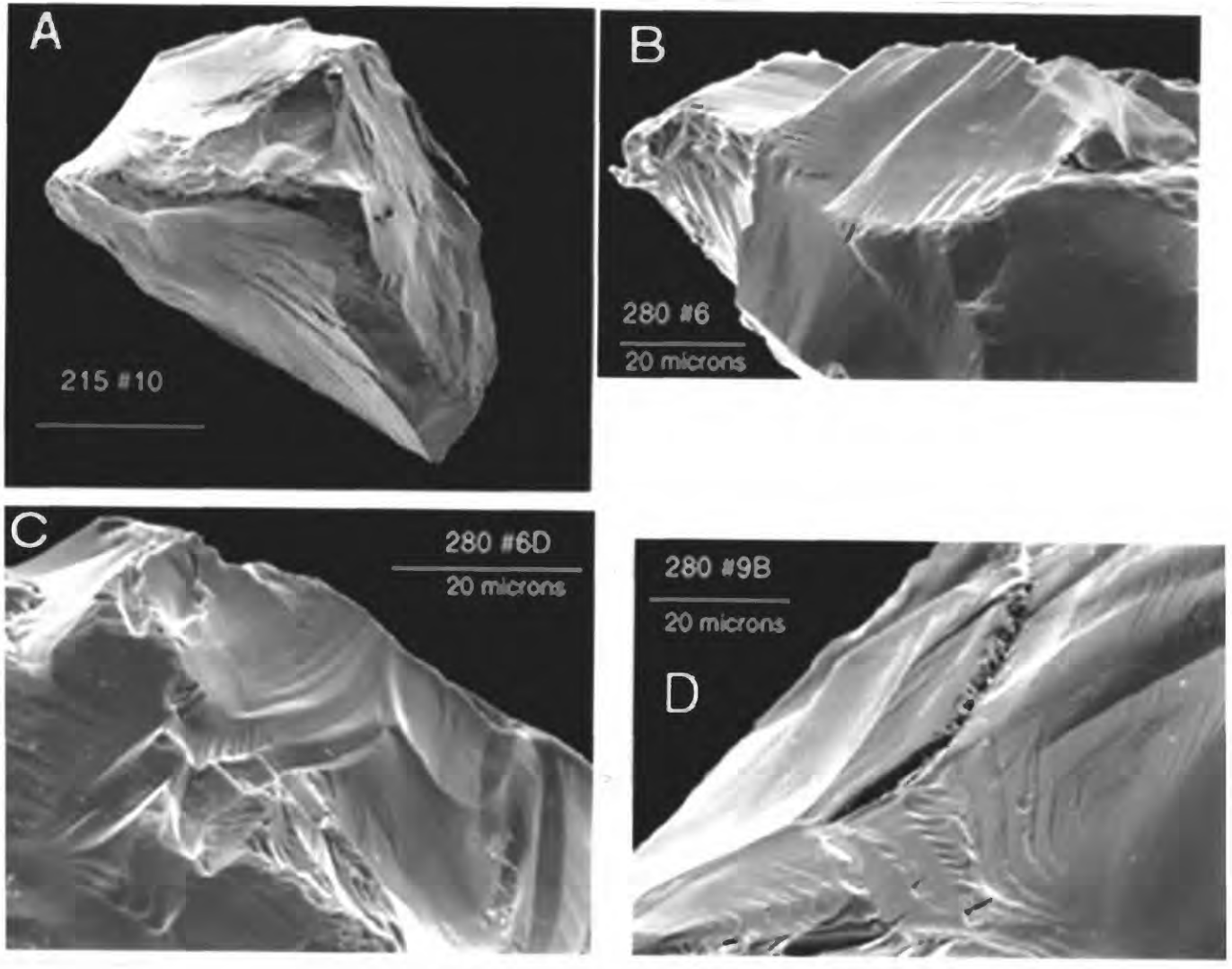

Plate 7: SEM images of close up of glacial features

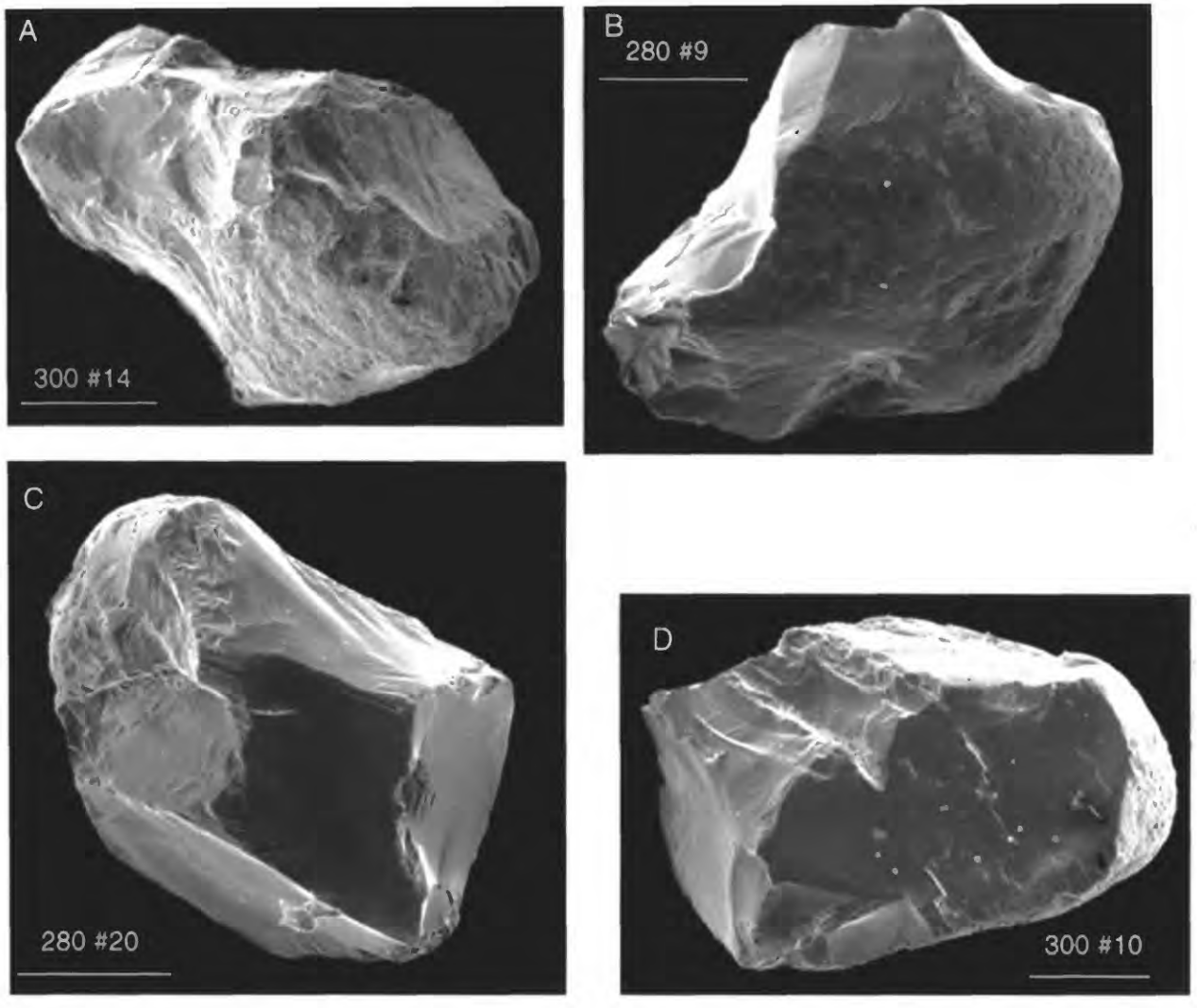

Plate 8: SEM images of type II grains (modified glacial grains)

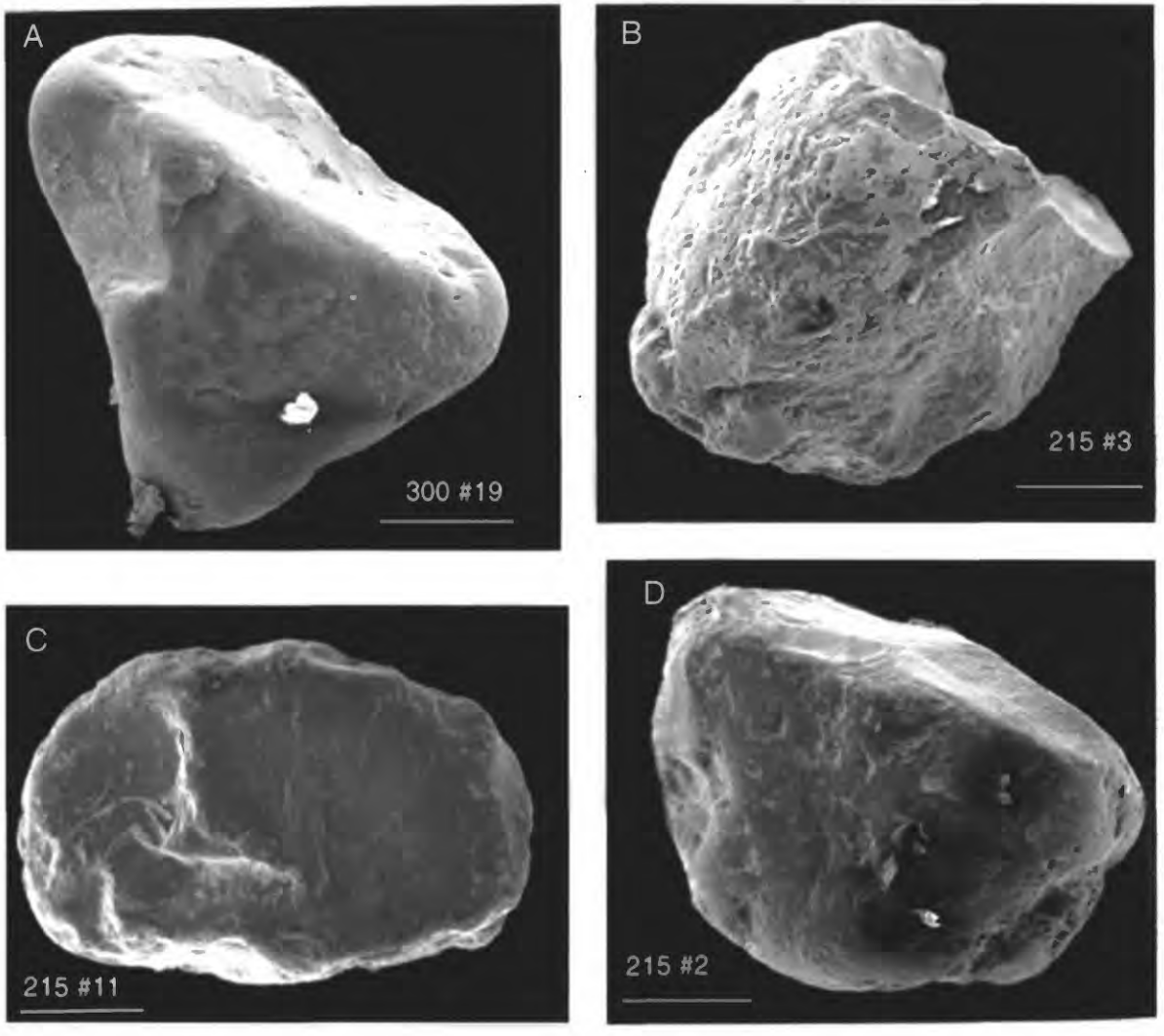

Plate 9: SEM images of type III grains (modified sea-ice grains)

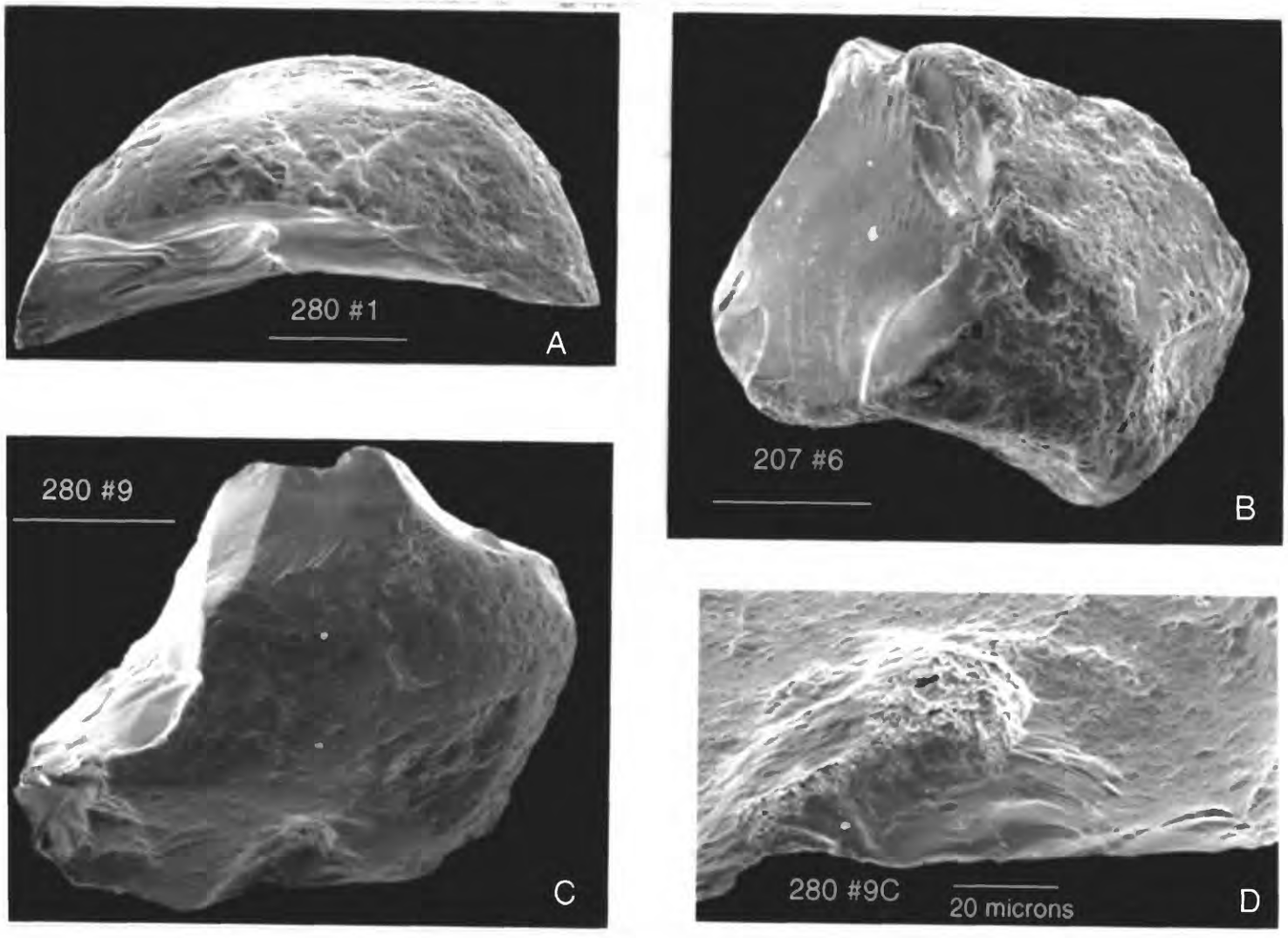

Plate 10: SEM images of reworked grains

Sample # 207-1	Grains																
Surface Feature	**1**	**2**	**3**	**4**	**5**	**6**	**7**	**8**	**9**	**10**	**11**	**14**	**15**	**16**	**19**	**20**	**AVE**
Mechanical Features:																	
high/med/low relief	2	3	3	1	3	3	3	3	3	3	3	3	3	3	3	3	**2.8**
small breakage blocks (<1 micron)	1	0	0	0	0	0	0	0	0	0	3	0	0	2	0	0	**0.4**
large breakage blocks (>1 micron)	1	0	0	0	0	0	0	0	0	0	3	0	0	2	0	0	**0.4**
small conchoidal fracture (<1 micron)	1	2	0	2	0	2	0	0	0	0	0	2	0	0	0	0	**0.6**
large conchoidal fracture (>1 micron)	2	2	0	2	0	2	0	0	0	0	0	2	0	0	0	0	**0.6**
fractured grain	2	0	0	2	0	0	0	0	0	0	0	2	0	0	0	0	**0.4**
step like fractures (II and sub-II)	1	2	0	0	0	0	0	0	0	0	0	1	0	0	0	0	**0.3**
arc step-like fractures	0	0	0	2	0	2	0	0	0	0	0	1	0	0	0	0	**0.3**
broken cleavage plates	0	0	0	0	0	0	0	0	0	0	3	0	0	2	0	0	**0.3**
grain embayment	0	0	0	0	0	0	0	0	0	0	0	0	0	0	0	0	**0.0**
crystalline node	0	0	0	0	0	0	0	0	0	0	0	0	0	0	0	0	**0.0**
diameter (x-axis) microns	394	269	424	359	350	389	380	424	382	362	292	487	369	318	241	491	**370.7**
diameter (y-axis) microns	449	314	282	451	377	383	414	296	365	367	259	485	432	284	278	362	**362.4**
Impact Features:																	
upturned plates	0	0	3	0	3	0	3	3	3	3	0	0	2	2	3	3	**1.8**
straight scratches (grooves)	0	0	0	0	0	0	0	0	0	0	0	0	2	0	0	2	**0.3**
curved scratch (grooves)	2	0	0	0	0	0	0	0	0	0	0	1	2	0	0	2	**0.4**
mechanical V's - impact pits	0	0	0	0	0	2	2	2	0	3	0	0	3	2	0	2	**1.0**
abraded surface	0	0	0	0	0	0	0	0	0	2	0	0	0	2	0	0	**0.3**
dish shaped concavities	0	0	2	0	0	0	0	0	2	0	0	0	2	2	2	2	**0.8**
shape (round, sub-r, sub-a, angular)	3	3	4	3	4	3	4	4	3	4	3	2	4	3	4	4	**3.4**

Appendix 1: Complete surface feature data

Sample # 207-1	Grains																
Surface Feature	**1**	**2**	**3**	**4**	**5**	**6**	**7**	**8**	**9**	**10**	**11**	**14**	**15**	**16**	**19**	**20**	**AVE**
Chemical Features:																	
oriented v-shaped etching	O	O	O	O	O	O	O	O	O	O	0	0	0	0	0	0	**0.0**
etching pits	O	O	O	O	O	O	O	O	O	O	3	3	3	3	2	2	**1.0**
silica precipitation	2	2	2	2	2	2	2	2	2	2	3	3	3	3	3	3	**2.4**
irregular pitted surface	2	2	2	2	2	2	2	2	2	2	3	3	3	3	3	3	**2.4**
crystal overgrowth	O	O	O	O	O	O	O	O	O	O	0	0	0	0	0	0	**0.0**

Shape	**Surface features**	**Relief**
Angular =1	none=0	high=1
sub-angular=2	present=1	medium=2
sub-round=3	common=2	low=3
round=4	abundant=3	

Appendix 1: Complete surface feature data

Sample # 215-1	Grains															
Surface Feature	**1**	**2**	**3**	**4**	**6**	**7**	**9**	**10**	**11**	**12**	**13**	**14**	**17**	**19**	**20**	**AVE**
Mechanical Features:																
high/med/low relief	2	3	3	3	3	3	3	1	3	3	2	3	3	3	3	**2.7**
small breakage blocks (<1 micron)	1	0	2	0	0	0	0	0	0	0	0	0	0	0	0	**0.2**
large breakage blocks (>1 micron)	2	2	2	0	0	0	0	0	0	0	0	0	0	0	0	**0.4**
small conchoidal fracture (<1 micron)	2	1	0	0	0	0	0	3	1	0	2	0	0	0	0	**0.6**
large conchoidal fracture (>1 micron)	2	1	0	0	0	0	0	3	1	0	2	0	1	0	0	**0.7**
fractured grain	2	0	0	0	0	0	0	3	1	0	1	0	0	0	0	**0.5**
step like fractures (II and sub-II)	2	0	0	0	0	0	0	0	1	0	1	0	0	0	0	**0.3**
arc step-like fractures	2	0	0	0	0	0	0	0	1	0	1	0	0	0	0	**0.3**
broken cleavage plates	2	1	0	0	0	0	0	0	0	0	0	0	0	0	0	**0.2**
grain embayment	0	0	0	0	0	0	0	0	0	0	0	0	0	0	0	**0.0**
crystalline node	0	0	0	0	0	0	0	0	0	0	0	0	0	0	2	**0.1**
diameter (x-axis) microns	567	362	346	342	327	342	406	384	285	350	291	385	415	420	330	**370.1**
diameter (y-axis) microns	403	333	359	319	279	381	385	422	475	440	444	319	395	425	298	**378.5**
Impact Features:																
upturned plates	2	2	3	3	3	3	3	0	0	3	1	2	3	3	3	**2.3**
straight scratches (grooves)	0	0	0	0	0	0	0	0	0	0	0	0	0	0	0	**0.0**
curved scratch (grooves)	0	0	0	3	0	?	0	0	0	0	0	3	0	0	0	**0.4**
mechanical V's - impact pits	?	1	2	3	0	3	?	0	2	0	2	3	1	1	1	**1.5**
abraded surface	?	0	0	0	0	?	0	0	0	0	2	0	0	0	0	**0.2**
dish shaped concavities	0	0	0	1	0	2	0	0	0	0	2	0	1	1	1	**0.5**
shape (round, sub-r, sub-a, angular)	2	4	3	4	4	4	4	1	3	3	3	4	3	4	3	**3.3**

Appendix 1: Complete surface feature data

Sample # 215-1	Grains															
Surface Feature	**1**	**2**	**3**	**4**	**6**	**7**	**9**	**10**	**11**	**12**	**13**	**14**	**17**	**19**	**20**	**AVE**
Chemical Features:																
oriented v-shaped etching	0	3	2	2	0	3	3	0	0	3	3	3	2	3	2	**1.9**
etching pits	2	3	2	3	3	3	3	0	1	3	3	3	3	3	3	**2.5**
silica precipitation	2	3	2	3	3	3	3	0	2	3	3	3	3	3	3	**2.6**
irregular pitted surface	2	3	2	3	0	0	?	0	0	3	3	3	3	3	3	**2.0**
crystal overgrowth	0	0	0	0	0	0	0	0	0	0	0	0	0	0	0	**0.0**

Shape	**Surface features**	**Relief**
Angular =1	none=0	high=1
sub-angular=2	present=1	medium=2
sub-round=3	common=2	low=3
round=4	abundant=3	

Appendix 1: Complete surface feature data

Sample #P26280	Grains															
Surface Feature	**1**	**2**	**3**	**4**	**5**	**6**	**7**	**9**	**11**	**12**	**13**	**14**	**15**	**16**	**20**	**AVE**
Mechanical Features:																
high/med/low relief	2	1	1	1	2	1	2	1	3	1	3	1	1	2	1	**1.5**
small breakage blocks (<1 micron)	0	0	0	0	0	0	0	0	0	0	0	1	3	0	0	**0.3**
large breakage blocks (>1 micron)	1	3	3	3	0	2	0	0	0	2	0	3	3	0	3	**1.5**
small conchoidal fracture (<1 micron)	0	0	0	0	0	0	0	0	0	2	0	1	3	2	1	**0.6**
large conchoidal fracture (>1 micron)	2	0	0	0	0	2	2	2	0	3	0	1	3	2	3	**1.3**
fractured grain	2	1	0	1	0	3	1	1	0	3	0	3	3	2	3	**1.5**
step like fractures (II and sub-II)	2	3	2	2	0	3	1	2	0	3	0	1	3	0	3	**1.7**
arc step-like fractures	2	0	0	0	0	3	3	2	0	3	0	1	3	0	3	**1.3**
broken cleavage plates	3	3	3	2	0	2	1	0	0	3	1	1	3	2	3	**1.8**
grain embayment	0	0	0	0	0	0	0	0	0	0	0	0	0	0	0	**0.0**
crystalline node	0	0	0	0	0	0	0	0	0	0	0	0	0	0	0	**0.0**
diameter (x-axis) microns	232	232	289	362	350	283	348	368	357	455	395	271	500	280	329	**336.7**
diameter (y-axis) microns	403	385	278	353	360	374	263	399	397	385	250	204	390	359	258	**337.2**
Impact Features:																
upturned plates	2	0	2	2	3	0	2	2	2	0	3	0	1	3	1	**1.5**
straight scratches (grooves)	0	0	0	0	0	0	0	0	?	0	0	0	0	0	0	**0.0**
curved scratch (grooves)	0	0	0	0	0	0	1	0	2	0	0	0	2	3	0	**0.5**
mechanical V's - impact pits	0	2	0	2	2	2	2	0	3	0	2	2	2	3	0	**1.5**
abraded surface									?	0	0	?	0	3	0	**0.6**
dish shaped concavities	0	0	0	0	0	0	0	0	0	0	0	0	0	1	0	**0.1**
shape (round, sub-r, sub-a, angular)	2	1	2	2	3	1	3	2	4	1	4	2	1	3	2	**2.2**

Appendix 1: Complete surface feature data

Sample #P26280	Grains															
Surface Feature	**1**	**2**	**3**	**4**	**5**	**6**	**7**	**9**	**11**	**12**	**13**	**14**	**15**	**16**	**20**	**AVE**
Chemical Features:																
oriented v-shaped etching	0	0	1	0	0	0	0	0	0	0	0	0	0	0	0	**0.1**
etching pits	0	2	0	2	0	0	0	0	3	0	3	2	1	3	0	**1.1**
silica precipitation	2	2	2	2	3	0	0	3	3	0	2	2	0	3	1	**1.7**
irregular pitted surface	2	2	2	2	3	0	2	0	3	0	2	2	0	3	0	**1.5**
crystal overgrowth	0	0	0	0	0	0	0	0	0	0	0	0	0	3	0	**0.2**
	Shape				**Surface features**						**Relief**					
	Angular =1				none=0						high=1					
	sub-angular=2				present=1						medium=2					
	sub-round=3				common=2						low=3					
	round=4				abundant=3											

Appendix 1: Complete surface feature data

Sample # P26 300	Grains													
Surface Feature	**1**	**2**	**3**	**4**	**5**	**6**	**9**	**10**	**14**	**16**	**18**	**19**	**20**	**AVE**
Mechanical Features:														
high/med/low relief	3	2	1	1	1	2	1	1	1	3	2	3	3	**1.8**
small breakage blocks (<1 micron)	0	0	0	0	3	0	0	0	0	0	0	0	0	**0.2**
large breakage blocks (>1 micron)	0	0	3	2	3	0	0	0	0	0	0	0	0	**0.6**
small conchoidal fracture (<1 micron)	0	3	1	3	2	1	3	2	3	3	2	0	0	**1.8**
large conchoidal fracture (>1 micron)	0	3	1	3	2	1	3	2	3	3	2	0	0	**1.8**
fractured grain	0	2	1	3	2	1	3	3	3	3	1	0	0	**1.7**
step like fractures (II and sub-II)	0	2	1	3	0	2	3	2	2	0	0	0	0	**1.2**
arc step-like fractures	0	2	0	3	0	2	3	0	2	3	0	0	0	**1.2**
broken cleavage plates	0	2	0	2	0	2	0	0	0	0	0	0	0	**0.5**
grain embayment	0	0	0	0	0	0	0	0	0	0	0	0	0	**0.0**
crystalline node	0	0	0	0	0	0	0	0	0	0	0	0	0	**0.0**
diameter (x-axis) microns	368	299	361	275	250	287	328	336	291	450	305	330	285	**320.4**
diameter (y-axis) microns	330	295	331	252	298	277	371	386	455	392	240	378	344	**334.5**
Impact Features:														
upturned plates	3	2	0	0	2	0	0	2	2	0	3	3	3	**1.5**
straight scratches (grooves)	0	0	0	0	0	0	0	0	0	0	0	0	0	**0.0**
curved scratch (grooves)	0	0	0	0	0	0	0	0	0	0	2	0	0	**0.2**
mechanical V's - impact pits	?	0	0	3	1	0	0	0	2	0	0	0	0	**0.5**
abraded surface	0	0	0	0	0	0	0	0	0	0	0	0	0	**0.0**
dish shaped concavities	0	0	0	0	0	0	0	0	0	0	0	0	0	**0.0**
shape (round, sub-r, sub-a, angular)	4	3	3	2	3	3	2	3	2	2	2	3	4	**2.8**

Appendix 1: Complete surface feature data

Sample # P26 300	Grains													
Surface Feature	**1**	**2**	**3**	**4**	**5**	**6**	**9**	**10**	**14**	**16**	**18**	**19**	**20**	**AVE**
Chemical Features:														
oriented v-shaped etching	3	0	3	0	2	2	0	0	0	0	0	3	3	**1.2**
etching pits	3	2	3	1	2	2	0	1	2	2	0	3	3	**1.8**
silica precipitation	3	2	3	0	2	2	0	1	2	0	3	3	3	**1.8**
irregular pitted surface	3	2	3	0	2	2	0	0	2	0	3	3	3	**1.8**
crystal overgrowth	0	0	0	0	2	0	0	0	0	0	0	0	0	**0.2**
	Shape				**Surface features**						**Relief**			
	Angular =1				none=0						high=1			
	sub-angular=2				present=1						medium=2			
	sub-round=3				common=2						low=3			
	round=4				abundant=3									

Appendix 1: Complete surface feature data